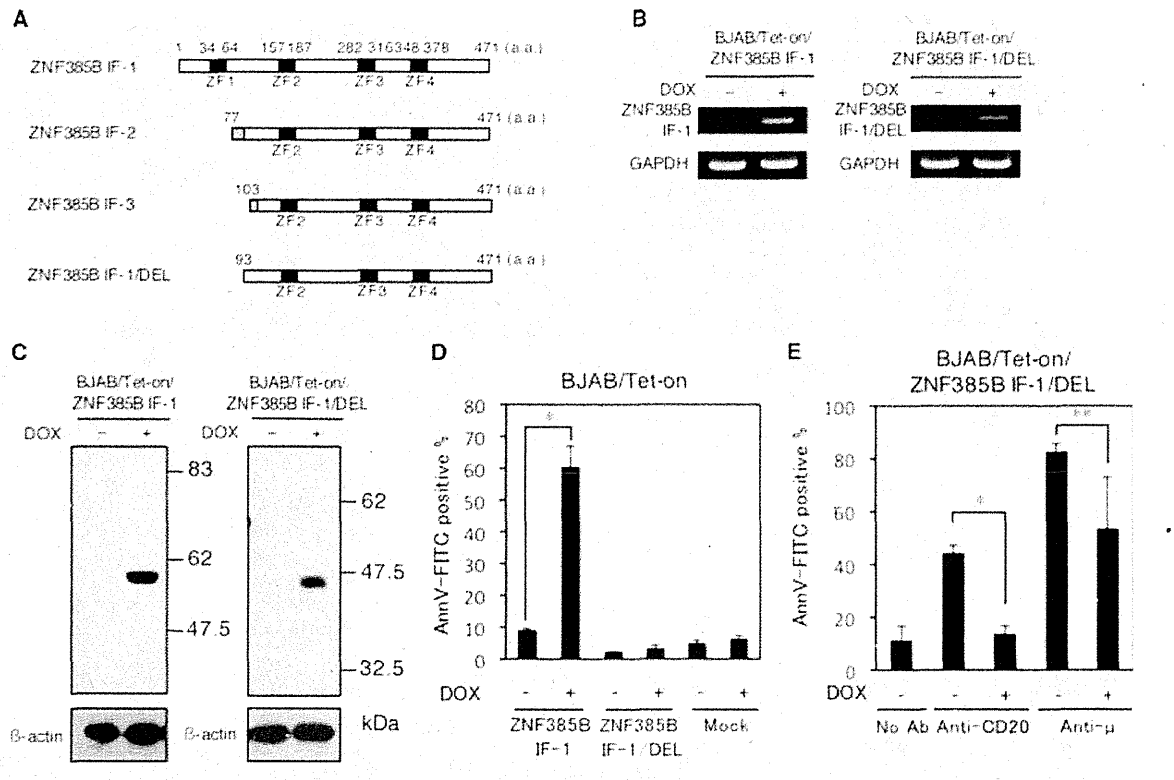

Figure 2. The effect of ZNF385B expression in BJAB cells. (A) Schematic representation of transcript variants of ZNF385B and constructed mutant. (B) The Tet-on inducible expression of *ZNF385B IF-1* and *IF-1/DEL* genes in BJAB transfectants was confirmed by RT-PCR. The cells were treated with or without 1 μg/mL DOX for the indicated periods. As an internal control, human *GAPDH* gene was also detected. (C) The ZNF 385B IF-1 and IF-1/DEL proteins were detected by immunoblot analysis in the same sample specimens as in (B). As an internal control, human β-actin was also detected. (B, C) Data shown are representative of at least three independent experiments performed. (D) BJAB Tet-on ZNF385B IF-1 and IF-1/DEL cells were treated with or without DOX for 96 h and apoptotic cells were identified by binding with FITC-labeled Annexin V (AnnV-FITC). The y-axis represents the ratio of AnnV-FITC-positive cells. As a negative control, BJAB Tet-on cells transfected with empty control vector (Mock) were simultaneously tested. (E) BJAB Tet-on ZNF385B IF-1/DEL cells were treated with or without DOX for 24 h followed by treatment with anti-CD20 and anti-mouse IgG Abs or anti-μ Ab for 48 h. Apoptotic cells were identified as in (D). (D, E) Data are shown as mean + SEM of triplicates and are representative of at least three independent experiments performed. $^{*}p < 0.01$; $^{**}p < 0.05$, compared with control using Student's *t*-test.

the longest transcript variant possessing four ZF domains, while ZNF385B IF-1/DEL corresponds to shorter isoforms IF-2/3 possessing three ZF domains and have high homology with ZNF385A. Inducible expression of both ZNF385B IF-1 and IF-1/DEL in BJAB cells was confirmed by RT-PCR and immunoblot analysis (Fig. 2B and C). We have also confirmed that more than 90% of cells expressed ZNF385B IF-1 by immunohistochemistry (data not shown). We then examined the effect of ZNF385B expression on apoptosis and found that DOX-mediated ectopic expression of ZNF385B IF-1 itself induced apoptosis in 96 h in BJAB cells as assessed by binding of AnnexinV-FITC (Fig. 2D). In contrast, when ZNF385B IF-1/DEL and control vector were similarly examined, no significant apoptosis was occurred in BJAB cells (Fig. 2D), indicating the specific effect of ZNF385B IF-1 on apoptosis induction. We also examined another ZNF385B-negative cell line MD901 and observed identical results, indicating that the effect of ZNF385B on apoptosis modulation does not specifically occur in BJAB cells but is common in ZNF385B-negative B-cell lines.

We also examined the effect of ZNF385B expression on apoptosis induced by Ab-mediated BCR and CD20 stimulation. Although 48 h of incubation with anti-μ and anti-CD20 Abs induced apoptosis in BJAB cells, DOX-mediated expression of ZNF385B IF-1 did not significantly affect apoptosis (data not shown). However, it is noteworthy that the expression of ZNF385B IF-1/DEL relieved apoptosis mediated by BCR and CD20 stimulation (Fig. 2E).

Next, we investigated the molecular basis of apoptosis mediated by ZNF385B IF-1 expression. When we examined the alteration of mitochondrial transmembrane potential by employing MitoCapture™ Apoptosis Detection Kit, ectopic expression of ZNF385B IF-1 caused fluorescence shift from red to green, indicating the disruption of the mitochondrial transmembrane potential (Fig. 3A). Furthermore, activation of caspase-3 and -8 was induced after induction of ZNF385B IF-1 (Fig. 3B).

Effect of ZNF385B on the expression of genes transactivated by p53

Since ZNF385A, which has high homology with ZNF385B IF2/3, is reported to affect the expression of genes transactivated by p53

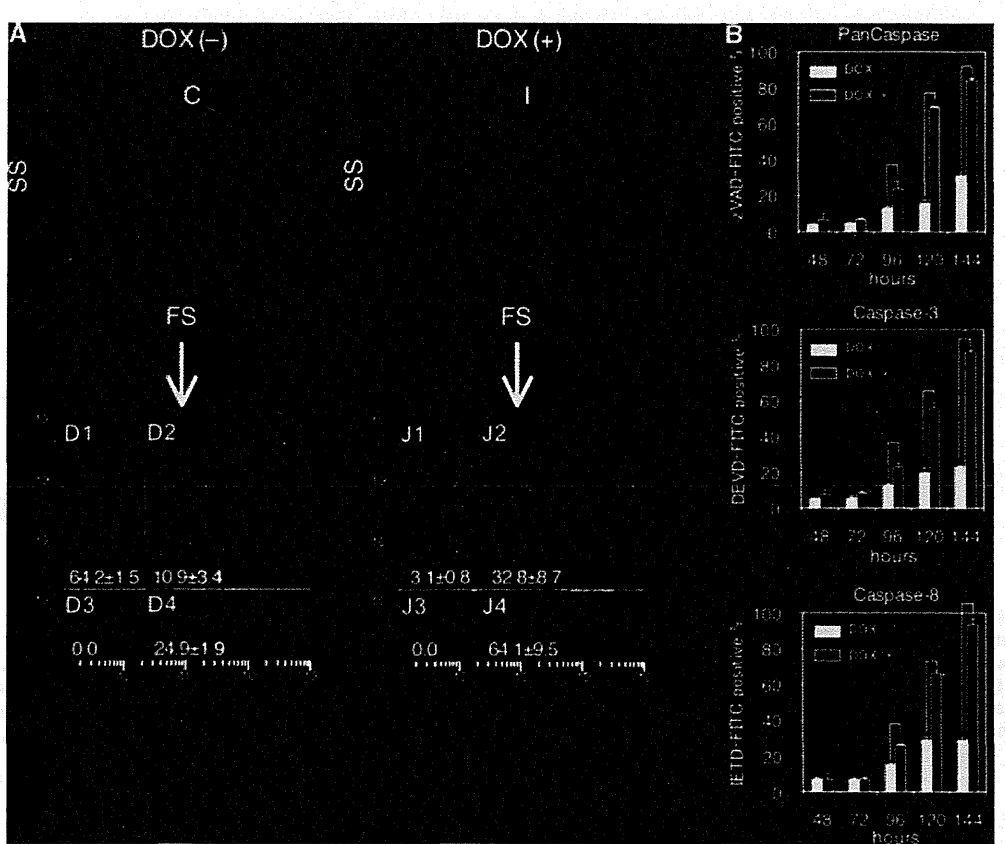

Figure 3. Analysis on ZNF385B IF-1-mediated apoptosis. (A) Mitochondrial transmembrane potential in BJAB transfectants treated with or without DOX for 6 days was determined using the MitoCapture Mitochondrial Apoptosis Detection Kit. The cationic dye MitoCapture was used to test the disruption of mitochondrial membrane potential. In the side scatter (SS) versus forward scatter (FS) plots, cells were gated by regions C and I. In viable cells, the dye aggregates in mitochondria and produces red fluorescence (FL2, y-axis), whereas in cells with altered membranes, it remains in the cytoplasm in monomeric form and produces green fluorescence (FL1, x-axis). The regions D4 and J4 represent the cell population with disrupted membrane potential. Representative plots are shown from three independent experiments. The experiment was performed in triplicate, and the means ± SEM of percentage for each region of a quadrant are presented. (B) The activation of pancaspase, caspase-3 and caspase-8 after DOX treatment for the indicated periods was detected by flow cytometry. The y-axis represents the ratio of zVAD-, DEVD-, and IETD-FITC-positive cells, respectively. Data are shown as mean + SEM of triplicates and are representative of at least three independent experiments. $^{*}p < 0.01$, $^{**}p < 0.05$, compared with control using Student's t-test.

[10], we then examined the effect of ZNF385B on the expression of some of apoptosis-related genes regulated by p53 [12] using real-time RT-PCR. As shown in Fig. 4A, the expression of ZNF385B IF-1 increased *PERP* and *FAS/CD95* expression, but not that of *BAX*, *BCL2*, *BIM*, *NOXA*, *p53TG1*, *14–3-3 σ*, *BCL6*, *PUMA*, or *CDKN1A* (Supporting Information Fig. 2). In contrast, ZNF385B IF-1/DEL did not affect the expression of PERP and *FAS/CD95* (Fig. 4A). Increased PERP expression was also confirmed at the protein level as assessed by immunoblot analysis (Fig. 4B). Furthermore, we observed that shRNA-mediated knockdown of *PERP* partially inhibited apoptosis induced by ZNF385B IF-1 expression (Fig. 4C, Supporting Information Fig. 3).

We next tested whether ZNF385B interacts with p53. For this purpose, BJAB Tet-on ZNF385B IF-1 cells treated with DOX for 48 h were lysed and immunoprecipitation was performed using p53-specific mAb. As shown in Fig. 5A, we observed that ZNF385B IF-1 was coimmunoprecipitated with p53, indicating the immunocomplex formation of ZNF385B IF-1 and p53. We further investigated the direct interaction between ZNF385B and p53 by means of a yeast two-hybrid assay. When ZNF385B protein fused to the Gal4 DNA-binding domain (pAS2–1-ZNF385B IF-1 and pAS2–1-ZNF385B IF-1/DEL) and p53 DNA-binding domain fused to the Gal4 transactivation domain (pACT2-p53) were coexpressed in Y187 yeast strain, both ZNF385B IF1 and ZNF385B IF-1/DEL induced colored colonies (Fig. 5B), indicating direct interaction between ZNF385B and p53.

Discussion

In this study, we demonstrated that the expression of ZNF385B is limited to a subset of GC B cells and their tumor counterpart BL cells among hematopoietic cells. Analysis using online available raw gene expression data indicated that *ZNF385B* was expressed only in $CXCR4^{+}$, but not $CXCR4^{-}$, tonsil B cells (Supporting Information Fig. 1). Since Caron et al. [11] demonstrated that

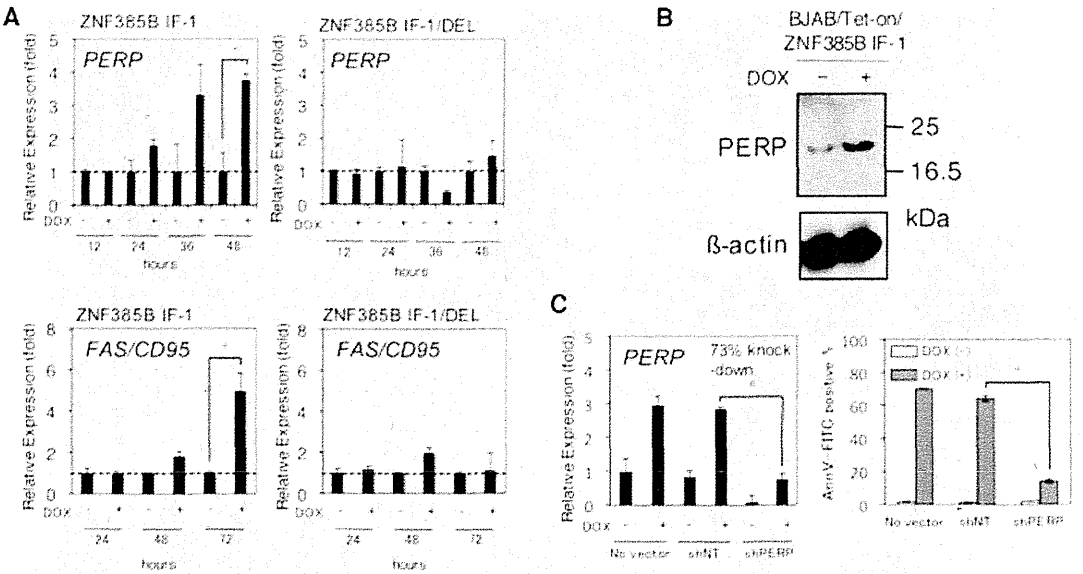

Figure 4. The expression of ZNF385B IF-1 increased PERP expression. (A) The expression analysis of p53 downstream genes (*PERP* and *FAS/CD95*) after DOX treatment was performed by real-time RT-PCR analysis using BJAB Tet-on ZNF385B IF-1 and IF-1/DEL cells. Signal intensity was normalized using that of a control housekeeping gene (human *GAPDH* gene). The y-axis represents the relative expression to that of DOX-negative cells. Data are shown as mean + SEM of triplicates and are representative of three independent experiments. * $p < 0.05$, compared with control using Student's t-test. Error bars indicate SEM. (B) The protein expression of PERP in the same sample specimens as in (A) was detected by immunoblot analysis. Actin served as a loading control. Data shown are representative of three experiments performed. (C) BJAB Tet-on ZNF385B IF-1 cells were transfected with *PERP* shRNA vector and the knockdown efficiency of *PERP* message by shRNA was assessed by real-time RT-PCR (the left panel). Then the cells were treated with or without DOX for 96 h and apoptotic cells were identified by binding with FITC-labeled Annexin V (AnnV-FITC) as presented in the right panel. As a negative control, BJAB Tet-on ZNF385B IF-1 cells and BJAB Tet-on ZNF385B IF-1 cells were transfected with nontarget shRNA vector (NT) and simultaneously tested. The y-axis represents the ratio of AnnV-FITC-positive cells; data are shown as mean + SEM of triplicates and are representative of three independent experiments.

CXCR4 expression could properly separate human centroblasts expressing activation-induced cytidine deaminase from centrocytes, it is suggested that ZNF385B was specifically expressed in centroblasts but not centrocytes. Furthermore, the ectopic expression of ZNF385B modulates the apoptotic induction in B cells. Interestingly, ZNF385B IF-1, the longest transcript variant, mediated apoptosis induction by itself but deletion mutant corresponding to ZNF385B IF-2/3, the shorter transcript variants, inhibited apoptosis induced by CD20 cross-linking and BCR stimulation in B cells.

ZNF385A, which has high homology with ZNF385B IF-2/3, was reported to be a p53-inducible gene product that is induced in response to genotoxic and oncogenic stress and inhibits the maintenance of G2 phase arrest following ionizing radiation, thereby sensitizing cells to DNA damage [13, 14]. In addition, ZNF385A was further reported to determine cell survival upon genotoxic stress by modulating p53 transactivation in an autoregulatory feedback loop [10]. Considering these findings together with our data, ZNF385A and B might be a protein family involved in p53-related DNA damage checkpoint machinery. Since we observed the absent expression of *ZNF385A* in peripheral lymphoid organs, ZNF385B possibly plays a role in the regulation of sensitization of GC B cells to DNA damage mediated by somatic hypermutation and immunoglobulin class switch recombination.

It is generally accepted that the expression of p53 in GC B cells is suppressed by BCL6 to allow toleration of the physiological DNA breaks required for somatic hypermutation and class switch recombination without inducing a p53-dependent apoptotic response [15], whereas complete loss of p53 function should increase the risks of the generating unintended autoreactive clones and oncogenic mutations. Margalit et al. [16] demonstrated that BCL6 transcription is positively regulated by p53, postulating that p53 is activated in response to the breaks formed in the genomic DNA due to somatic hypermutation and class switch recombination in GC B cells, and p53-mediated BCL6 expression forms an autoregulatory loop to modulate p53 function. Actually, our data indicate the expression of p53 in a subset of B cells in peripheral lymph nodes. Therefore, interdependent regulation of p53 and BCL6 functions should play a crucial role in appropriate control for clonal expansion and clonal deletion of GC B cells. In this context, ZNF385B should be involved in the regulatory machinery of p53 function and contribute to clonal selection of GC B cells. Further studies to elucidate the role of ZNF385B in the development of GC B cells are now under way.

As we also presented, the expression of ZNF385B IF-1 activated caspase-8 and -3 and disrupted the mitochondrial membrane potential. Caspase-8 was found to be mainly activated by death receptor apoptotic signaling, such as Fas/CD95 and TNFRs [17], whereas p53-mediated upregulation of PERP also led to increased levels of cleaved caspase-8 forms, as well as to reduction of its full-length substrate Bid [18]. Caspase-3 is in the downstream signaling pathway of caspase-8 and known to be an effector caspase. As

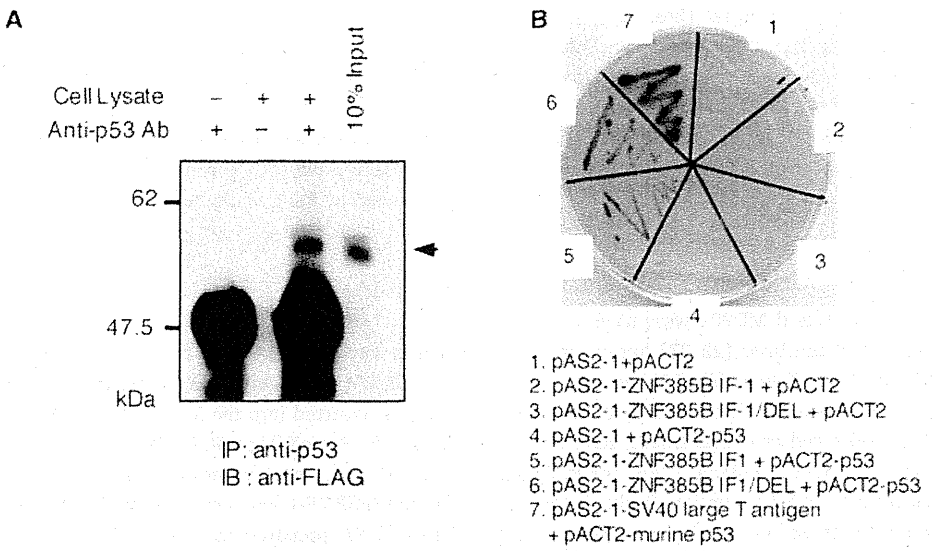

Figure 5. Binding of ZNF385B with p53. (A) Immunoprecipitation (IP) and Western blot analysis of BJAB Tet-on ZNF385B IF-1 treated with 1 μg/mL DOX for 48 h were performed using anti-p53 Ab and anti-Flag Ab, respectively. The bands corresponding to ZNF385B IF-1 protein are indicated by an arrow. (B) Yeast two-hybrid assay to show direct interaction between ZNF385B IF-1 and p53. Yeast two-hybrid assay was performed using the combination of plasmids as indicated. The colored colony formation indicates the binding between the proteins introduced into the yeasts. Representative data are shown from at least three independent experiments.

we observed upregulation of *PERP* and *FAS/CD95*, these molecules are candidate mediators of ZNF385B IF-1-induced activation of caspase-8. Indeed, our data that partial inhibition of ZNF385B IF-1 induced apoptosis by *PERP* knockdown mediated by shRNA (Fig. 4C) indicate the involvement of PERP in the apoptotic process. Since the transcription of both *PERP* and *FAS/CD95* is regulated by p53 [12], it is reasonable to speculate that ZNF385B directly modulates p53 transactivation for *PERP* and *FAS/CD95*, resulting in caspase-8 activation. The fact that FAS/CD95 is reported to be required for clonal selection within GC and establishment of the memory B-cell repertoire [19] and B-lymphocyte homeostasis [20] should support the notion of involvement of ZNF385B-mediated *FAS/CD95* upregulation in GC B-cell development.

As mentioned above, ZNF385B has both proapoptotic and antiapoptotic activities depending on the type of isoform. Since both longest and shorter isoforms can bind to p53 (Fig. 5B), the additional ZF domain located at the *N*-terminus of IF-1 (Fig. 2A) should confer opposite function to shorter isoforms, although the precise mechanism involved is still under investigation. They might act together as a dominant-negative system in the regulation of p53 function and are involved in the apoptotic regulation of GC B cells.

Although healthy lymphoid tissue mainly expressed IF-2/3, some BL cell lines predominantly expressed IF-1 (Fig. 1C). Since high expression of proapoptotic IF-1 seems to be disadvantageous for tumor genesis, predominant expression of IF-1 in BL cell lines looks inconsistent. However, considering this together with the fact that loss and inactivation of p53 proteins mediated by gene mutations are frequently observed in BL cells [21], it can be speculated that the cell origin of BL cells is GC centroblasts destined for elimination by negative selection, but that acquire resistance to apoptosis.

In conclusion, zinc-finger protein ZNF385B characteristically expressed in GC B cells had both proapoptotic and antiapoptotic activities depending on the type of isoform. ZNF385B IF-1 directly interacts with p53 and induces apoptosis via upregulation of PERP and *FAS/CD95*, followed by activation of caspase-8 and caspase-3. Although further analysis to elucidate the function of ZNF385B is clearly needed, our observation should shed light on the functional role of this zinc finger protein in the course of B-cell development in GCs.

Materials and methods

Reagents

Mouse and rabbit polyclonal Abs against ZNF385B (Sigma-Aldrich, St. Louis, MO, cat # SAB1408384, and ABGENT, San Diego, CA, cat # AP5790b, respectively) were used. The mouse mAbs used for the immunohistochemical and the biochemical analysis were anti-CD20 from Dako (Glostrup, Denmark), anti-BCL6 from Leica Biosystems Newcastle Ltd. (Newcastle, UK, cat # NCL-BCL-6), anti-actin from Sigma-Aldrich, anti-FLAG from Invitrogen (Carlsbad, CA), and anti-p53 (Bp53–12) from Santa Cruz Biotechnology, Inc. (Santa Cruz, CA). The Rabbit mAbs used for the immunohistochemical analysis was anti-active caspase-3 from BD Biosciences (San Jose, CA). Purified anti-μ chain rabbit polyclonal Ab from Jackson Immuno Research Laboratories Inc. (West Grove, PA) was used to cross-link BCRs. Mouse

anti-CD20 mAbs from Beckman Coulter (Brea, CA) were used to cross-link CD20. Secondary Abs, including enzyme-conjugated Abs and biotin-conjugated Abs, were purchased from Jackson, Dako and Vector Laboratories Inc. (Burlingame, CA). Retrovirus vectors for shRNA targeting *PERP* were obtained from Takara Bio Inc. (Shiga, Japan).

Cells and materials

The human B-cell lines BJAB and MD901 were used. Both were first reported as BL-derived cell lines [22, 23] but are later considered to be DLBCL-derived cell lines [24, 25] because of a lack of myc translocation [26]. Another human DLBCL-derived cell line SU-DHL-4 [27], BL-derived cell lines Daudi, Raji, P32/ISH (Japanese Cancer Research Resource Bank, JCRB, Tokyo, Japan), EB-3, NAMALWA (Institution of Fermentation, Osaka, Japan), CA-46 (Dainippon Pharmacology Co., Osaka, Japan), BALM-18 [28], BALM-24 [29], hairy cell leukemia-derived cell line MLMA (JCRB), multiple myeloma-derived cell line IM-9 [30], B-cell precursor acute lymphoblastic leukemia-derived cell line Reh (American Type Culture Collection), P30/OHK (JCRB), NALM-17, NALM-27 (Research Center Cell Biology Institute, Hayashibara Biochemical Laboratories, INC., Okayama, Japan), NALM-6 (Tohoku University Cell Bank, Sendai, Japan), LC4–1, T acute lymphoblastic leukemia-derived cell line CCRF-CEM, acute myeloid leukemia-derived cell line K562, and EOL-1 (JCRB) were used. Cells were cultured at 37°C in RPMI 1640 medium (Sigma-Aldrich Corp., St. Louis, MO), supplemented with 10% FCS (Thermo Fisher Scientific Inc., Waltham, MA), under a humidified 5% CO_2 atmosphere. The transformed embryonal kidney cell line 293FT (Invitrogen) was also used and cultured in DMEM (Sigma-Aldrich). For Tet-inducible system, Tet system-approved FBS (Clontech Laboratories, Inc., Mountain View, CA) was used.

Clinical specimens from pediatric patients, including nontumorous mononuclear cells separated from autopsied spleen of a patient with myelodysplastic syndrome, nontumorous tonsil, and formalin-fixed, paraffin-embedded tissue specimens from nontumorous reactive lymphadenitis, were used. The specimens have been collected between 1985 and 2001 at our laboratory and are now kept under conditions of anonymity. All of the experiments included in this study followed the tenets of the Declaration of Helsinki and were performed with the approval of the local ethics committee. In the case of splenic mononuclear cells, $CD20^+$ B cells were sorted using EPICS ALTRA (Beckman) and then RNA was extracted.

MTC Multiple Tissue cDNA Panels were obtained from Clontech. MVPTM total RNA, human lymph node, was obtained from Stratagene Co. (La Jolla, CA).

Immunohistochemistry

For immunohistochemical staining, the formalin-fixed, paraffin-embedded tissue specimens were deparaffinized, treated using the heat-induced epitope retrieval method in 10 mM citrate buffer, pH 6.0, or 1 mM EDTA, pH 8.0, stained with Abs using the avidin-biotin complex system and visualized with DAB. In the case of double staining with anti-ZNF385B and anti-CD20 or anti-cleaved caspase-3, visualizations with NovaRED and DAB-Ni (Vector Laboratories, inc., Burlingame, CA), respectively, were used as instructed by the manufacturer.

Plasmid construction

A gateway cassette (bases 1–1705) was amplified from pBLOCK-iT3-DEST (Invitrogen) with FLAG-tag by PCR, and the PCR product was inserted into the *Eco*RV site of pRetroX-Tight (Clontech) (termed pRetroX Tight-FLAG-DEST). Full-length (IF-1) and partially deleted (corresponding to AA93 to 471, IF-1/DEL) cDNA of *ZNF385B* IF-1 was amplified with primers shown in Table 1 from cDNA prepared from EB-3 cells by PCR using KOD plus ver.2 (Toyobo Co., Ltd., Osaka, Japan) and cloned into the *Xmn*I-*Eco*RV sites of pENTR11 (Invitrogen). The resulting pENTR11-ZNF385B IF-1 and pENTR11-ZNF385B IF-1/DEL were recombined with pRetroX Tight-FLAG-DEST using an LR recombination reaction as instructed by the manufacturer (Invitrogen) to construct the tetracycline-inducible *ZNF385B* expression vector pRetroX Tight-FLAG-ZNF385B. Amplified *ZNF385B* IF-1 cDNA and *ZNF385B* IF-1/DEL with primers shown in Table 1 were also inserted into pGEMT easy vector (Promega Co., Fitchburg, WI) and subcloned into the *Eco*RI site of pAS2–1 (Clontech), termed pAS2–1-ZNF385B IF-1 and pAS2–1-ZNF385B IF-1/DEL, respectively. Amplified *p53* cDNA was inserted into pGEMT easy vector (Promega) and subcloned into the *Eco*RI site of pACT2, termed pACT2-p53.

Transfection and induction of ZNF385B

293FT cells were seeded at a density of 5×10^6 cells per 10-cm culture dish 1 day prior to transfection. Retroviral vectors (25 μg), together with pCL gag-pol (22.5 μg) and pCMV VSV-G (2.5 μg), were cotransfected into 293FT cells with Fugene HD (Roche, Penzberg, Germany) and incubated overnight as previously described [31]. After 24 h of incubation, the medium containing virus was collected, filtered through 0.45-μm filters (Millipore, Bedford, MA) and then centrifuged at 6000 × *g* for 16 h. Supernatant was removed and viral pellet was diluted with 4 mL of fresh medium containing 5 ng/μL polybrene (Sigma-Aldrich). Typically, 5×10^5 cells in a well of a 6-well plate were infected with 2 mL of viral solution of each gene. After 24 h, the medium was replaced with fresh medium and selected in the medium containing appropriate antibiotics. The Tet-on advanced-introduced cells were further infected with retrovirus of pRetroX Tight FLAG-ZNF385B IF-1 and IF-1/DEL. The transfectants were treated with 1 μg/mL doxycycline (DOX) for the indicated period. Induced expression of ZNF385B in transfectants was confirmed by RT-PCR and immunoblotting. Knockdown of *PERP* in BJAB Tet-on

Table 1. The sequences of gene-specific primers for RT-PCR and real-time RT-PCR used in this study

Name of gene	Forward primer	Reverse primer
ZNF385B (common)	ccaggccgaggcccactaca	actcgggctccgctggagtt
ZNF385B (cloning, IF-1)	atgaatatggcaaattttctacggggcttt	ttagtacggagcaaagaggatggaggcagg
ZNF385B (Y2H cloning, IF-1)	gatgaatatggcaaattttctacggggcttt	ttagtacggagcaaagaggatggaggcagg
ZNF385B (cloning, DEL)	atgcttcctgctcttgtgcgcacacctacc	ttagtacggagcaaagaggatggaggcagg
ZNF385B (Y2H cloning, DEL)	gatgcttcctgctcttgtgcgcacacctacc	ttagtacggagcaaagaggatggaggcagg
ZNF385B (qPCR, IF-1)	gggctaacctggaaaccga	tcagctgacaggaatttggaca
ZNF385B (qPCR, IF-2)	cgtggtgctgtcacacaga	ggataatgcacagcgctacc
ZNF385B (qPCR, IF-3)	gggctaacctggaaaccga	gcacaagagcaggaagggta
ZNF385B (qPCR control vector, IF-1)	gggctaacctggaaaccga	ctcagctgcttcactcgtttgc
ZNF385B (qPCR control vector, IF-2)	agcggcactgatataacgtggtgc	gtgatggagcagctgggattagcct
ZNF385B (qPCR control vector, IF-3)	cgtgaacgtggactgtaaccttaaaaacaaa ggcagtacatgccacacta	gcacaagagcaggaagggtagtagtgtggcatg tactgcctttgttttta
p53 (Full)	gtggcccctgtcatcttctgtcccttccca	tcagggcagctcgtggtgaggctccccttt
PERP	taccttaacggcgcacattt	tggttctattatatcaggctcgttg
BAX	gtggcagctgacatgttttc	caaagtagaaaagggcgacaa
CDKN1A	atgtgtcctggttcccgtttc	cattgtgggaggagctgtga
14–3-3σ	gacacagagtccggcattg	atggctctggggacacac
Fas/CD95	tgaaggacatggcttagaagtg	cacttggtgttgctggtgag
BCL2	ttgtggccttctttgagttcggtg	ggtgccggttcaggtactcagtca
BIM	tggcaaagcaaccttctgatg	gcaggctgcaattgtctacct
PUMA	aagagcaaatgagccaaacg	aaacgagccccactctctg
BCL6	agcaaggcattggtgaagaca	atggcgggtgaactggatac
P53TG1	gcaggtctggcttaccaca	gtgtaagtgttcgcctggtg
NOXA	cagctgtccgaggtgctc	ccgcccactcagctacag
GAPDH (qPCR control vector)	aaattgagcccgcagcctcccgcttcgctc	ggttgagcacagggtactttattgatggta
GAPDH (RT-PCR)	ccacccatggcaaattccatggca	tctagacggcaggtcaggtccacc
GAPDH (qPCR)	gctcagacaccatggggaaggt	gtggtgcaggaggcattgctga

ZNF385B IF-1 cells using retroviral vector-mediated shRNA was performed similarly to that described above.

Detection of apoptosis

The incidences of apoptosis were quantified by using FITC-labeled Annexin V of MEBCYTO-Apoptosis kit (Medical & Biological Laboratories Co., Ltd., MBL, Nagoya, Japan). After each treatment indicated in the figure legends, 2.5×10^5 BJAB transfectants were collected and incubated with Annexin V-FITC in 500 μL of binding buffer for 5 min at room temperature according to the manufacturer's protocol [32].

The incidences of apoptosis were also quantified by using MitoCapture™ Mitochondrial apoptosis detection kit (MBL). After each treatment indicated in the figure legends, 1.0×10^6 BJAB transfectants were collected and resuspended in 1 mL of the diluted MitoCapture solution and incubated at 37°C in a 5% CO_2 incubator for 15 min according to the manufacturer's protocol [32].

Activation of pancaspase, caspase-3 and caspase-8 were quantified using an APOPCYTO Intracellular Caspase Activity Detection Kit (MBL). After each treatment indicated in the figure legends, 2.5×10^5 BJAB transfectants were collected and incubated with FITC-VAD-FMK, FITC-DEVD-FMK, and FITC-IETD-FMK, for 30–60 min at 37°C in CO_2 incubator.

Data were collected on a FC500 flow cytometer (Beckman) and were analyzed with CXP software (Beckman). Fluorescence-minus-one was used to assess background fluorescence for each population.

PCR

Total RNA was extracted from cultured cells with an Illustra RNAspin (GE Healthcare Bio-Sciences UK Ltd., Chalfont, UK), and cDNA was generated with a First Strand cDNA Synthesis Kit (GE) and ReverTra Ace-α (Toyobo). The set of primers used in this study is shown in Table 1.

Real-time RT-PCR was performed using power SYBR Green PCR Master Mix on an ABI PRISM 7900HT Sequence Detection System (Applied Biosystems, Carlsbad, CA) according to the manufacturer's instructions. The human *GAPDH* gene was used as an internal control for normalization. The set of primers used for real-time PCR is also shown in Table 1. The vector controls of *ZNF385B* isoforms and *GAPDH* were constructed by subcloning of PCR amplicons into pGEMT and pENTR11 (*Xmn*I and *Eco*RV site) vectors, respectively.

Immunoprecipitation and immunoblotting

Cell extracts were prepared and immunoprecipitations were performed using 1 mg cell extracts as described previously [33]. It was confirmed that the cell extracts contain nuclear p53 by immunoblotting (data not shown). Whole cell extracts were incubated with anti-p53 Ab (Santa Cruz) bound to Protein A Mag Sepharose Xtra (GE). The bound complexes were collected by magnet, washed and separated by SDS-PAGE.

Immunoblotting was performed as described previously [33]. Briefly, a 50-μg sample of each cell lysate was electrophoretically separated on an SDS-polyacrylamide gel and transferred to a nitrocellulose membrane. The membrane was incubated with the appropriate combination of primary and secondary Abs, washed and examined with ECL Plus Western Blotting Detection System (GE).

Yeast two-hybrid assay

Yeast two-hybrid assay was performed following the manufacturer's protocol (Clontech). Briefly, pAS2–1-ZNF385B IF-1 vector and pAS2–1-ZNF385B IF-1/DEL vector were transformed into yeast strain Y187 with pACT2-p53 and then plated on SD/-Trp/-Leu/X-Gal plates. Vector set pAS2–1-SV40 large T antigen and p-ACT2-murine p53 were used as positive control. Representative colonies for the samples, positive control and negative controls were streaked onto an SD/-Trp/-Leu/X-Gal plate.

Statistical analysis

Data were analyzed using Student's *t*-test. Values of p less than 0.05 were considered statistically significant. All experiments were performed at least three times and means and SEM were calculated.

Acknowledgments: The plasmids pCL gag-pol and pCMV VSV-G were kindly provided by Dr. Tohru Kiyono, National Cancer Research Center. K.I. is awardee of Research Resident Fellowship from the Foundation for Promotion of Cancer Research (Japan) for the 3rd Term Comprehensive 10-Year Strategy for Cancer Control. This work was supported by a grant from Health and Labour Sciences Research Grants (the 3rd-term comprehensive 10-year strategy for cancer control H22–011), the Japan Health Sciences Foundation for Research on Publicly Essential Drugs and Medical Devices (KHA1002), the Grant of National Center for Child Health and Development (22A-5), Grant-in-Aid for Young Scientists (B) (23791211), and the Advanced research for medical products Mining Programme of the National Institute of Biomedical Innovation (NIBIO, 10-45).

Conflict of interest: The authors declare no financial or commercial conflict of interest.

References

1 Gatto, D. and Brink, R., The germinal center reaction. *J. Allergy Clin. Immunol.* 2010. 126: 898–907.

2 Goodnow, C. C., Vinuesa, C. G., Randall, K. L., Mackay, F. and Brink, R., Control systems and decision making for antibody production. *Nat. Immunol.* 2010. 11: 681–688.

3 Levine, M. H., Haberman, A. M., Sant'Angelo, D. B., Hannum, L. G., Cancro, M. P., Janeway, C. A. Jr and Shlomchik, M. J., A B-cell receptor-specific selection step governs immature to mature B cell differentiation. *Proc. Natl. Acad. Sci. USA* 2000. 97: 2743–2748.

4 Hanley-Hyde, J. M. and Lynch, R. G., The physiology of B cells as studied with tumor models. *Annu. Rev. Immunol.* 1986. 4: 621–649.

5 Gregory, C. D., Tursz, T., Edwards, C. F., Tetaud, C., Talbot, M., Caillou, B., Rickinson, A. B. et al., Identification of a subset of normal B cells with a Burkitt's lymphoma (BL)-like phenotype. *J. Immunol.* 1987. 139: 313–318.

6 Kiyokawa, N., Kokai, Y., Ishimoto, K., Fujita, H., Fujimoto, J. and Hata, J. I., Characterization of the common acute lymphoblastic leukaemia antigen (CD10) as an activation molecule on mature human B cells. *Clin. Exp. Immunol.* 1990. 79: 322–327.

7 Mangeney, M., Lingwood, C. A., Taga, S., Caillou, B., Tursz, T. and Wiels, J., Apoptosis induced in Burkitt's lymphoma cells via Gb3/CD77, a glycolipid antigen. *Cancer Res.* 1993. 53: 5314–5319.

8 Bellan, C., Lazzi, S., Hummel, M., Palummo, N., de Santi, M., Amato, T., Nyagol, J. et al., Immunoglobulin gene analysis reveals 2 distinct cells of origin for EBV-positive and EBV-negative Burkitt lymphomas. *Blood* 2005. 106: 1031–1036.

9 Sharma, S., Dimasi, D, Higginson, K. and Della, N. G., RZF, a zinc-finger protein in the photoreceptors of human retina. *Gene* 2004. 342: 219–229.

10 Das, S., Raj, L., Zhao, B., Kimura, Y., Bernstein, A., Aaronson, S. A. and Lee, S. W., Hzf determines cell survival upon genotoxic stress by modulating p53 transactivation. *Cell* 2007. 130: 624–637.

11 Caron, G., Le Gallou, S., Lamy, T., Tarte, K. and Fest, T., CXCR4 expression functionally discriminates centroblasts versus centrocytes within human germinal center B cells. *J. Immunol.* 2009. 182: 7595–7602.

12 Attardi, L. D., Reczek, E. E., Cosmas, C., Demicco, E. G., McCurrach, M. E., Lowe, S. W. and Jacks, T., PERP, an apoptosis-associated target of p53, is a novel member of the PMP-22/gas3 family. *Genes Dev.* 2000. 14: 704–718.

13 Sugimoto, M., Gromley, A. and Sherr, C. J., Hzf, a p53-responsive gene, regulates maintenance of the G_2 phase checkpoint induced by DNA damage. *Mol. Cell. Biol.* 2006. 26: 502–512.

14 Nakamura, H., Kawagishi, H., Watanabe, A., Sugimoto, K., Maruyama, M. and Sugimoto, M., Cooperative role of the RNA-binding proteins Hzf and HuR in p53 activation. *Mol. Cell. Biol.* 2011. 31: 1997–2009.

15 Phan, R. T. and Dalla-Favera, R., The BCL6 proto-oncogene suppresses p53 expression in germinal-centre B cells. *Nature* 2004. 432: 635–639.

16 Margalit, O., Amram, H., Amariglio, N., Simon, A. J., Shaklai, S., Granot, G., Minsky, N. et al., BCL6 is regulated by p53 through a response element frequently disrupted in B-cell non-Hodgkin lymphoma. *Blood* 2006. 107: 1599–1607.

17 Boldin, M. P., Goncharov, T. M., Goltsev, Y. V. and Wallach, D., Involvement of MACH, a novel MORT1/FADD-interacting protease, in Fas/APO-1- and TNF receptor-induced cell death. *Cell* 1996. 85: 803–815.

18 Davies, L., Gray, D., Spiller, D., White, M. R., Damato, B., Grierson, I. and Paraoan, L., P53 apoptosis mediator PERP: localization, function and caspase activation in uveal melanoma. *J. Cell. Mol. Med.* 2009. 13: 1995–2007.

19 Takahashi, Y., Ohta, H. and Takemori, T., Fas is required for clonal selection in germinal centers and the subsequent establishment of the memory B cell repertoire. *Immunity* 2001. 14: 181–192.

20 Hao, Z., Duncan, G. S., Seagal, J., Su, Y. W., Hong, C., Haight, J., Chen, N. J. et al., Fas receptor expression in germinal-center B cells is essential for T and B lymphocyte homeostasis. *Immunity* 2008. 29: 615–627.

21 Farrell, P. J., Allan, G. J., Shanahan, F., Vousden, K. H. and Crook, T., p53 is frequently mutated in Burkitt's lymphoma cell lines. *EMBO J.* 1991. 10: 2879–2887.

22 Menezes, J., Leibold, W., Klein, G. and Clements, G., Establishment and characterization of an Epstein-Barr virus (EBC)-negative lymphoblastoid B cell line (BJA-B) from an exceptional, EBV-genome-negative African Burkitt's lymphoma. *Biomedicine* 1975. 22: 276–284.

23 Miki, T., Kawamata, N., Arai, A., Ohashi, K., Nakamura, Y., Kato, A., Hirosawa, S. et al., Molecular cloning of the breakpoint for 3q27 translocation in B-cell lymphomas and leukemias. *Blood* 1994. 83: 217–222.

24 Lenz, G., Davis, R. E., Ngo, V. N., Lam, L., George, T. C., Wright, G. W., Dave, S. S. et al., Oncogenic CARD11 mutations in human diffuse large B cell lymphoma. *Science* 2008. 319: 1676–1679.

25 Sanchez-Izquierdo, D., Buchonnet, G., Siebert, R., Gascoyne, R. D., Climent, J., Karran, L., Marin, M. et al., MALT1 is deregulated by both chromosomal translocation and amplification in B-cell non-Hodgkin lymphoma. *Blood* 2003. 101: 4539–4546.

26 Glazer, P. M. and Summers, W. C., Oncogene expression in isogenic, EBV-positive and -negative Burkitt lymphoma cell lines. *Intervirology* 1985. 23: 82–89.

27 Epstein, A. L., Marder, R. J., Winter, J. N. and Fox, R. I., Two new monoclonal Abs (LN-1, LN-2) reactive in B5 formalin-fixed, paraffin-embedded tissues with follicular center and mantle zone human B lymphocytes and derived tumors. *J. Immunol.* 1984. 133: 1028–1036.

28 Matsuo, Y., Sugimoto, A., Harashima, A., Nishizaki, C., Ishimaru, F., Kondo, E., Katayama, Y. et al., Establishment and characterization of a novel ALL-L3 cell line (BALM-18): induction of apoptosis by anti-IgM and inhibition of apoptosis by bone marrow stroma cells. *Leuk. Res.* 1999. 23: 559–568.

29 Mimori, K., Kiyokawa, N., Taguchi, T., Suzuki, T., Sekino, T., Nakajima, H., Saito, M. et al., Costimulatory signals distinctively affect CD20- and B-cell-antigen-receptor-mediated apoptosis in Burkitt's lymphoma/leukemia cells. *Leukemia* 2003. 17: 1164–1174.

30 Fahey, J. L., Buell, D. N. and Sox, H. C., Proliferation and differentiation of lymphoid cells: studies with human lymphoid cell lines and immunoglobulin synthesis. *Ann. NY. Acad. Sci.* 1971. 190: 221–234.

31 Dias, J., Gumenyuk, M., Kang, H., Vodyanik, M., Yu, J., Thomson, J. A. and Slukvin, I. I., Generation of red blood cells from human induced pluripotent stem cells. *Stem Cells Dev.* 2011. 20: 1639–1647.

32 Matsui, J., Kiyokawa, N., Takenouchi, H., Taguchi, T., Suzuki, K., Shiozawa, Y., Saito, M. et al., Dietary bioflavonoids induce apoptosis in human leukemia cells. *Leuk. Res.* 2005. 29: 573–581.

33 Kiyokawa, N., Lee, E. K., Karunagaran, D., Lin, S. Y. and Hung, M. C., Mitosis-specific negative regulation of epidermal growth factor receptor, triggered by a decrease in ligand binding and dimerization, can be overcome by overexpression of receptor. *J. Biol. Chem.* 1997. 272: 18656–18665.

Abbreviations: BL: Burkitt's lymphoma · DLBCL: diffuse large B-cell lymphoma · DOX: doxycycline · IF: isoform · ZF: zinc finger

Full correspondence: Dr. Nobutaka Kiyokawa, Department of Pediatric Hematology and Oncology Research, National Research Institute for Child Health and Development, 2-10-1, Okura, Setagaya-ku, Tokyo 157-8535, Japan
Fax: +81-3-3417-2496
e-mail: nkiyokawa@nch.go.jp

Received: 14/3/2012
Revised: 8/8/2012
Accepted: 30/8/2012
Accepted article online: 4/9/2012

Biochimica et Biophysica Acta 1820 (2012) 1715–1723

Contents lists available at SciVerse ScienceDirect

Biochimica et Biophysica Acta

journal homepage: www.elsevier.com/locate/bbagen

The human CD10 lacking an *N*-glycan at Asn_{628} is deficient in surface expression and neutral endopeptidase activity

Ban Sato [a,1], Yohko U. Katagiri [a], Kazutoshi Iijima [a], Hiroyuki Yamada [a], Satsuki Ito [b], Nana Kawasaki [b], Hajime Okita [a], Junichiro Fujimoto [c], Nobutaka Kiyokawa [a,*]

[a] Department of Pediatric Hematology and Oncology Research, National Research Institute for Child Health and Development, 2-10-1 Okura, Setagaya-ku, Tokyo 157–8535, Japan
[b] Division of Biological Chemistry and Biologicals, National Institute of Health Science, 1-18-1 Kami-yoga, Setagaya-ku, Tokyo 158–8501, Japan
[c] Clinical Research Center, National Research Institute for Child Health and Development, 2-10-1 Okura, Setagaya-ku, Tokyo 157–8535, Japan

ARTICLE INFO

Article history:
Received 26 October 2011
Received in revised form 22 June 2012
Accepted 25 June 2012
Available online 3 July 2012

Keywords:
CD10
N-glycan
Neutral endopeptidase
Glycopeptidase F
Site-directed mutagenesis
Common acute lymphoblastic leukemia antigen (CALLA)

ABSTRACT

Background: CD10, also known as neprilysin or enkephalinase exhibiting neutral endopeptidase (NEP) activity, is expressed by B-lineage hematopoietic cells as well as a variety of cells from normal tissues. It cleaves peptides such as cytokines to act for terminating inflammatory responses. Although CD10 molecules of the human pre-B-cell line NALM-6 have 6 consensus *N*-glycosylation sites, three of them are known to be *N*-glycosylated by X-ray crystallography.
Methods: In order to investigate the role of *N*-glycans in the full expression of NEP activity, we modified *N*-glycans by treatment of NALM6 cells with various glycosidases or alter each of the consensus *N*-glycosylation sites by generating site-directed mutagenesis and compared the NEP activities of the sugar-altered CD10 with those of intact CD10.
Results: CD10 of the human B-cell line NALM-6 was dominantly localized in raft microdomains and heterogeneously *N*-glycosylated. Although neither desialylation nor further degalactosylation caused defective NEP activity, removal of only a small part of *N*-glycans by treatment with glycopeptidase F under non-denaturing conditions decreased NEP activity completely. All of the three consensus sites of CD10 in HEK293 cells introduced with wild type-CD10 were confirmed to be *N*-glycosylated. Surface expression of *N*-glycan at Asn_{628}-deleted CD10 by HEK293 cells was greatly decreased as well as it lost entire NEP activities.
Conclusions: *N*-glycosylation at Asn_{628} is essential not only for NEP activities, but also for surface expression.
General significance: Quality control system does not allow dysfunctional ecto-type proteases to express on plasma membrane.

1. Introduction

CD10 was initially reported to be expressed by "common" acute lymphoblastic leukemia (ALL) cells [1] and thus termed as the common acute lymphoblastic leukemia antigen (CALLA), whereas it was later found to be expressed by a variety of cells from normal tissues. For example, CD10 was shown to be expressed on CD179a/b$^+$ precursor-B-cells (a normal counterpart of "common"-ALL) in bone marrow [2] and early activated B-cells in the germinal center of peripheral lymphoid organs during normal B-cell development [3]. CD10 is transiently expressed during the development of not only hematopoietic lineages, but also multiple organs and stem cells in a variety of tissues, including mature granulocytes, renal epithelium, and myoepithelium [4,5].

Although the biological significance of CD10 is not fully clarified, it is known to be a type II transmembrane glycoprotein exhibiting NEP (EC 3.4.24.11) activity [6] and can cleave a number of biological active peptides such as substance P, endothelin, oxytocin, enkephalin, angiotensins [7], or amyloid-β-peptide [8] at the amino side of hydrophobic amino acids and reduces inflammatory responses or terminates signaling by degrading the ligands in peripheral tissues. In fact, CD10-targeted mice showed enhanced mortality upon galactosamine-sensitized endotoxin shock or treatment combining TNF-α and IL-1β [9]. The protease activity of CD10 has also been implicated in maintenance of homeostasis such as fluid balance and nervous system function [10]. Furthermore, in regulating human mammary stem cells, CD10 is proposed to create a gradient of signaling proteins by degrading those nearest to the basement membrane [11].

Raft microdomains provide a platform for a variety of cell functions including signal transduction and play a crucial role in cell development and differentiation [12,13]. We previously investigated apoptotic signal transduction of B-cell precursor ALL cells [14] and Burkitt's lymphoma cells [15] via raft microdomains by cross-linking of B-cell receptor or

* Corresponding author. Tel.: +81 3 3416 0181; fax: +81 43 226 2496.
E-mail address: nkiyokawa@nch.go.jp (N. Kiyokawa).
[1] Present address: Department of Biochemistry, Kobe Pharmaceutical University, 4-19-1 Motoyamakitamachi, Higashinada-ku, Kobe 658–8558, Japan.

0304-4165/$ – see front matter © 2012 Elsevier B.V. All rights reserved.
doi:10.1016/j.bbagen.2012.06.017

GPI-anchored molecules. Since CD10 of B-cell precursor ALL cell lines is recovered in raft microdomain fractions, it might be involved in signal transduction via raft microdomains, and NEP activity of CD10 might play an important role by terminating cell signaling. In an attempt to investigate the functional role of CD10 in B-cell precursor ALL cells, we examined the localization of CD10 in raft microdomain and its biochemical characteristics and observed that NEP activities of their CD10 molecules were suppressed by glycopeptidase F treatment. It is well known that glycosylation regulates the function of glycoproteins [16], so we used oligonucleotide-directed mutagenesis to alter each of the consensus *N*-glycosylation sites in human CD10 and examined the NEP activities of the wild type (WT) and mutated CD10 transiently expressed in HEK-293 cells. Although a human CD10 molecule has 6 consensus *N*-glycosylation sites, X-ray crystallography has shown that only 3 of them are *N*-glycosylated [17] (Fig. 1). We confirmed that all of these sites were *N*-glycosylated and found that *N*-glycosylation at Asn_{628} is essential not only for NEP activities, but also for surface expression.

2. Materials and methods

2.1. Cells and reagents

Pre-B ALL-derived cell line NALM-6, Pro-B ALL-derived cell line NALM-16 and Reh [2], and Burkitt's lymphoma-derived cell line RAMOS (Japanese Cancer Research Resource Bank, Tokyo, Japan) were cultured in RPMI 1640 supplemented with 10% FBS at 37 °C in a humidified 5% CO_2 atmosphere. The anti-human CD10 monoclonal antibodies (mAs) used were IF6, developed in our laboratory [18], and NCL-CD10-270, purchased from Novocastra Laboratories Ltd. (Newcastle-upon-Tyne, UK). The second antibodies used were HRP-conjugated rabbit anti-mouse IgG + M (DAKO) and FITC-conjugated goat anti-mouse IgG + M (Jackson Immunoresearch, West Grove, PA). HRP-conjugated RCA lectin was purchased from J-OIL MILLS (Seikagaku Corp., Tokyo, Japan).

2.2. Preparation of cytoplasmic and membrane fractions and raft microdomains

Biochemical subcellular fractionation of NALM-6 cells was carried out as previously described [19]. Briefly, cells were homogenized in a low ionic cell lysis buffer (25 mM NaCl/0.5 mM $MgCl_2$/18 mM Tris–HCl buffer, pH7.5) and cell debris was removed by centrifugation at 200 ×*g* for 5 min at 4 °C. The supernatant was centrifuged in a microcentrifuge at 15,000 rpm (19,270 ×*g*) for 30 min at 4 °C to separate supernatant and pellet as the cytoplasmic fraction and the total membrane fraction, respectively. The total membrane fraction was treated with 1% Triton X-100 in 0.15 M NaCl/25 mM Tris–HCl buffer, pH 7.5, for 30 min at 4 °C and centrifuged at 15,000 rpm for 30 min at 4 °C to separate supernatant and precipitate as the detergent-soluble and -insoluble fractions, respectively. Raft microdomains were obtained by ultracentrifugation of a suspension of the Triton-treated total membrane fraction in 40% sucrose as previously described [12]. Membranes or raft microdomains were solubilized in 40 μM heptylthioglucoside (Dojin Laboratories, Kumamoto, Japan)/1% Triton X-100/0.15 M NaCl/25 mM Tris–HCl buffer, pH 7.5, for 30 min at 4 °C and centrifuged at 15,000 rpm for 30 min at 4 °C to separate membrane lysates.

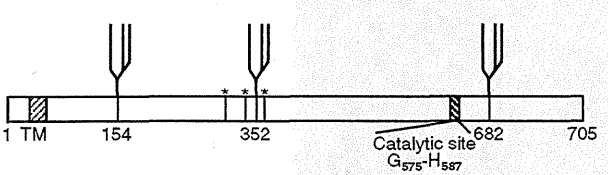

symbol	mutation
WT	wild type
Δ1	N145Q
Δ2	N325Q
Δ3	N628Q

Fig. 1. Schematic diagram of *N*-glycosylation sites in human CD10 and site-directed mutagenesis. TM, transmembrane domain; *, putative glycosylation sites, but confirmed to be unglycosylated by X-ray crystallography; ⇓ confirmed to be glycosylated. Symbols of mutants, in which Asn was substituted by Gln at the indicated sites, are shown.

2.3. PAGE and Western blot analysis

Proteins were separated in 10% polyacrylamide gels under reducing conditions after dissolving in a loading buffer containing 1.7% SDS and 0.1 M dithiothreitol. Two dimensional (2D) PAGE was performed using the Mini-PROTEAN II 2-D system (Bio-Rad Laboratories, Hercules, CA) as previously described [13]. Gels were either silver-stained or transferred onto PVDF membranes (Millipore Corporation, Bedford, MS). The blots were blocked with 5% skimmed milk in PBS and probed with NCL-CD10-270, then with HRP-conjugated anti-mouse IgG + M antibodies, or blocked with 3% BSA, then probed with HRP-conjugated RCA lectin.

2.4. LC/MS/MS of N-glycans

The spots of CD10 in a 2D separated gel were excised and cut into pieces. The gel pieces were destained and dehydrated with 50% acetonitrile. The protein in the gel was reduced and carboxymethylated by incubation with dithiothreitol and sodium monoiodoacetate [20]. *N*-glycans were extracted from the gel pieces as reported previously [21] and reduced with $NaBH_4$. The borohydride-reduced glycans were desalted with Envi-carb (Aldrich). LC/MS/MS was carried out as previously described [22]. A full MS scan (m/z 450–2000) in positive and negative ion modes by FT-ICR MS was followed by data-dependent MS/MS for the most abundant ion performed in the positive ion mode.

2.5. Assay of NEP activity

Enzyme sources of NEP to be examined were intact cells of pro- and pre-B-cell lines, raft microdomains, and CD10 purified by immunoprecipitation with anti-CD10 mAb IF6 bound to Protein A/agarose beads (Bio-Rad). Cells were extensively washed in phosphate-buffered saline (PBS) and resuspended at 1×10^5 cell/mL in the same buffer. Raft microdomains or purified CD10 bound to IF6/PA/agarose beads were suspended in PBS. NEP activity on intact cells or in raft microdomains and purified CD10 was fluorometrically assayed using an indirect coupled enzyme assay method [23]. 5×10^4 cells, raft microdomains, or CD10 on PA/agarose beads were incubated with 0.2 mM glutaryl-Ala-Ala-Phe-4-methyl-coumaryl-7-amides (MCA) (Peptide Institute, Osaka, Japan) at 37 °C for 30 min in 20 mM PBS (pH 7.0) in the presence or absence of 0.5 mM phosphoramidon (Peptide Institute), in a total volume of 50 μL. Subsequently, enzyme sources were removed from the reaction mixture by centrifugation. To the reaction mixture was then added 5 μL of a solution containing 0.1 mg (0.4 units equivalent)/mL leucine aminopeptidase (L-5006; Sigma, St. Louis, MO, USA) and 0.2 mM phosphoramidon, followed by further incubation for 30 min at 37 °C to remove a phenylalanine residue from Phe-MCA formed by NEP-catalyzed digestion. The intensity of the liberated 7-amino-4-methylcoumarin was measured at excitation 390 nm and emission 460 nm on a 96-well black plate (CORNING, Amsterdam, Netherlands) using a microplate spectrometer (ARVO, Perkin Elmer Inc., Waltham, MA). The NEP activity was determined on the basis of the decrease in the rate of digestion caused by 0.5 mM phosphoramidon. The relative

amount of CD10 was determined by Western blot analysis using LAS imaging analyzer (Fuji Film, Tokyo, Japan).

2.6. Glycosidase digestion

Raft microdomains or CD10 molecules on IF6-bound Protein A/agarose beads were incubated with 25 mU of sialidase (*Arthrobacter ureafaciens*, Nacalai Tesque, Kyoto, Japan) in 50 μL of 0.1 M sodium acetate buffer, pH 5.0, for 7 h at 37 °C, and then/or 25 mU of β-galactosidase (*Escherichia coli*, Sigma) in 50 μL of 0.1 M sodium phosphate buffer, pH 7.2/1 mM $MgCl_2$ for 13 h at 37 °C. Alternatively, they were incubated with 1 mU of recombinant glycopeptidase F (*Escherichia coli*, Takara, Tokyo, Japan) in 50 μL of native buffer or denaturing buffer according to the manufacturer's instructions overnight.

2.7. CD10 expression vector

The cDNA of the human CD10 was amplified by PCR from the reverse-transcribed product of total RNA from NALM-6 cells extracted using Illustra RNAspin Mini RNA Isolation Kit (GE Healthcare Bio-Science Corp.) and subcloned into the expression vector pcDNA3 (termed as pcDNA3-CD10). Mutations were introduced into the cDNA for CD10 using a QuickChange Site-Directed Mutagenesis kit (Stratagene, La Jolla, CA) according to the manufacturer's instructions. The coding regions of

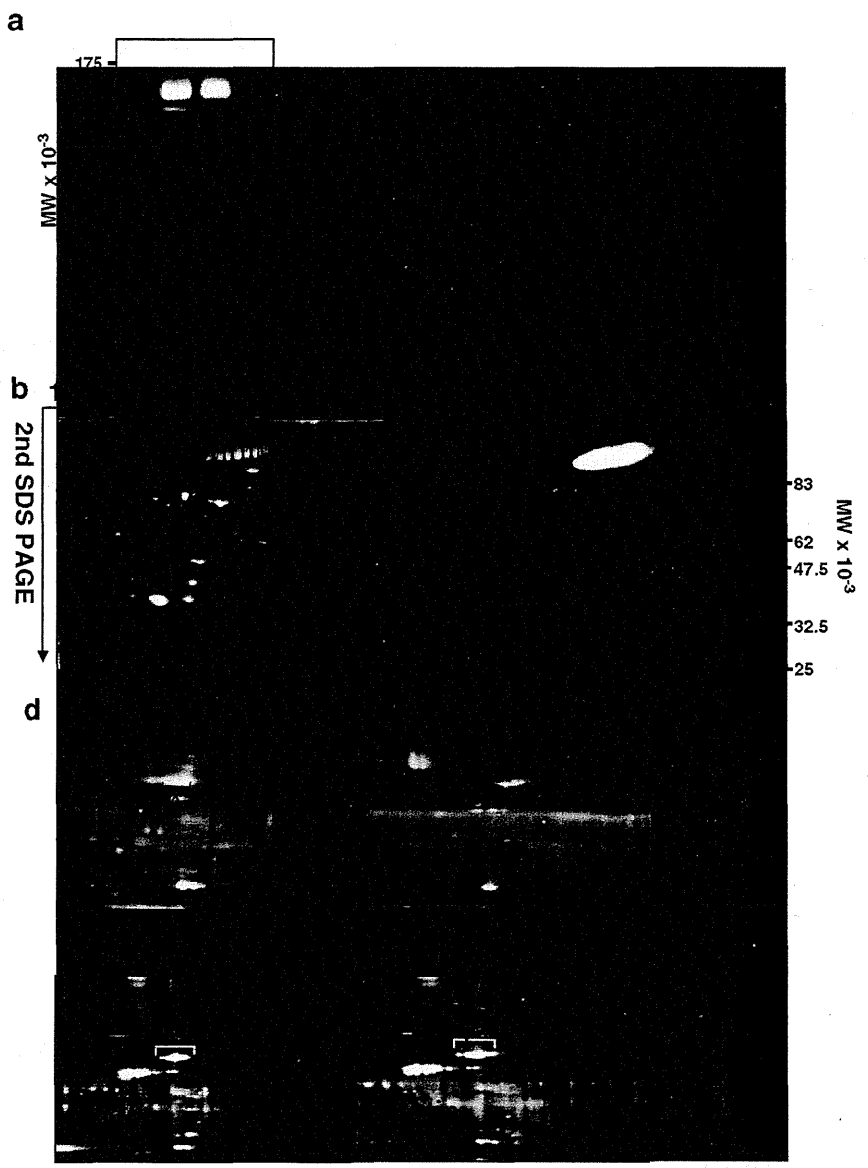

Fig. 2. Characterization of CD10 molecules expressed by human pre-B-cell line NALM-6. a, Distribution of CD10 molecules in cytoplasmic fraction, detergent-insoluble membrane fraction, and detergent-soluble membrane fraction of NALM-6 cells. Each lane contains proteins derived from 2.3×10^6 cells. b, 2D PAGE of NALM-6 raft microdomain. 60 μg of protein was subjected to 2D PAGE, and the 2D gel was stained with CBB. c, Immunostaining of the 2D separated raft microdomain with anti-CD10. 12 μg of protein was subjected to 2D PAGE. d, 2D PAGE of the glycosidase-treated raft microdomain. The raft microdomain (12 μg each) was treated with glycopeptidase F under denaturing conditions (upper left) or sialidase (upper right), and the glycopeptidase F-treated raft microdomain (lower left) was further treated with sialidase (lower right). The raft microdomains thus obtained were subjected to 2D PAGE, and the 2D gels were silver-stained. * and ** indicate de-*N*-glycosylated and desialylated CD10, respectively.

all constructs of cDNA for CD10 were sequenced using an ABI PRISM 3130 sequencer (Applied Biosystems Japan Ltd., Tokyo, Japan). Primers for amplifying, sequencing, and mutagenesis are listed in Table 2. The constructed vectors were transiently transfected into HEK293 cells using Lipofectamine™ LTX (Invitrogen) according to the manufacturer's directions. Cells were cultured for up to 3 days in the presence of 1.5 mg of G418 disulfate (Nacalai Tesque).

2.8. Flow cytometry

Harvested cells were incubated with IF6 for 30 min on ice, and then with FITC-conjugated goat anti-mouse IgG + M for a further 30 min on ice. Stained cells were analyzed using a Beckman Coulter Gallios (Beckman Coulter, Miami Lakes, FL). Five thousand cells were analyzed using FlowJo software (Treestar, Inc., San Carlos, CA).

2.9. RT-PCR

Total RNA was isolated from the transfected cells as described above. cDNA was synthesized from 5 μg of total RNA using a First-Strand cDNA Synthesis Kit (GE Healthcare Bio-Science Corp.). The sequences of gene-specific primers for RT PCR were as follows: for CD10 (forward), 5′-GGAAGAAAGATTGCCCATCG-3′; for CD10 (reverse), 5′-GAGGCTGCTTA CAAGATCCATTATG-3′; for GAPDH (forward), 5′-GCTCAGAACACCATG GGGAAGGT-3′; and for GAPDH (reverse), 5′-GTGGTGCAGGAGGCAT TGCTGA-3′.

2.10. Protein transport and degradation inhibitors treatment

Cells were cultured in the presence or absence of 5 μg/mL brefeldin A (Sigma) or 25 μM chloroqunie (Sigma) for 1 day and 10 μM lactacystin (Peptide Institute) for 2 days.

3. Results

3.1. Localization of NALM-6 CD10 in raft microdomains

The solubility of CD10 molecules for Triton X-100 detergent was examined by Western analysis. CD10 molecules having a molecular weight (MW) of 91 k~120 k were hardly recovered in the cytoplasmic fraction (Fig. 2a, lane 1), but were in the membrane fraction (lane 2), and 95% and 5% of membrane-bound CD10 were recovered in the detergent-insoluble fraction (lane 3) and detergent-soluble fraction (lane 4), respectively. A detergent-insoluble and low-density fraction, namely, raft microdomain, of NALM-6 cells was separated by 2D PAGE and stained with Coomassie brilliant blue (CBB) (Fig. 2b). Proteomic analysis of all spots enclosed by ovals revealed that the series of molecules with a wide range of isoelectric point (pI) from 4.9 to 5.3 was CD10. Anti-CD10 mAb specifically bound to these spots on a PVDF membrane to which 2D PAGE-separated raft molecules were transferred (Fig. 2c). Removal of *N*-glycans from CD10 molecules by digestion with glycopeptidase F under denaturing conditions reduced the molecular weight to 81 k and focused pI to the basic side (* in Fig. 2d, upper left), and sialidase treatment of CD10 molecules shifted the pI more to the basic side (** in Fig. 2d, upper right). Since further treatment of de-*N*-glycosylated CD10 with sialidase did not change the pI (Fig. 2d, lower left and right), all sialic acids are suggested to be on *N*-glycans. These results show that CD10 is a membrane glycoprotein having heterogeneously sialylated *N*-glycans.

3.2. Glycosylation analysis of NALM-6 CD10

The 2D PAGE gel containing the CD10 molecules was excised and treated with glycopeptidase F. The released *N*-glycans were subjected to LC/MS/MS^n. Fig. 3 shows the oligosaccharide profile obtained by a full mass scan (m/z 450~2000) in the positive and negative ion

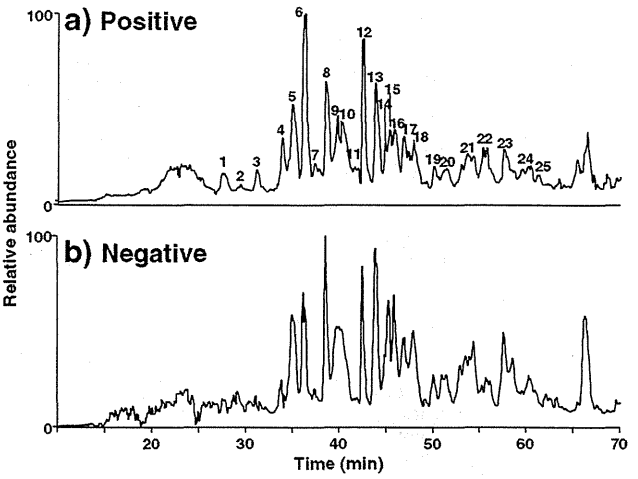

Fig. 3. Total ion current chromatograms of *N*-glycans released from NALM-6 CD10. a, Positive ion mode. b, Negative ion mode.

modes. The most abundant ion in each scan was automatically subjected to data-dependent collision-induced dissociation-MS/MS. Deduced oligosaccharide structures and compositions estimated on the basis of measured accurate masses are summarized in Table 1. Although only three sites of N_{145}, N_{325}, and N_{628} of 6 potential *N*-glycosylation sites are known to be glycosylated [24], more than 46 oligosaccharide chains were detected. LC-MS analysis revealed that CD10 possesses extremely heterogeneous *N*-glycans.

3.3. NEP activities of surface-expressed CD10 of human B-cell lines

NEP activities of CD10 expressed by human pro-B-cell line Reh and NALM-16, pre-B-cell line NALM-6, and Burkitt's lymphoma RAMOS were measured using fluorogenic substrate, and are expressed as nmol MCA released in a 50 μL test volume for 30 min. Although NEP activities per 5×10^4 cells varied with cell lines, specific activities, which were defined as MCA released (nmol) per CD10 arbitrary unit, were almost the same (Fig. 4).

3.4. Effects of glycosidase treatment of CD10 on NEP activities

In order to investigate the role of oligosaccharide chains for the expression of NEP catalytic activity, we digested raft microdomains of NALM-6 cells or purified CD10 with glycopeptidase F under non-denaturing conditions, sialidase, and/or β-galactosidase, and measured the NEP activity.

The MW of CD10 of NALM-6 cells treated with sialidase was slightly reduced (Fig. 5a, lane 2). Treatment with glycopeptidase F under non-denaturing conditions did not reduce the MW of CD10 (lane 3), whereas extensive digestion under denaturing conditions reduced it to 81 k (lane 4). Disappearance of acidic and high MW area of glycopeptidase F-treated CD10 under non-denaturing conditions in a 2D-PAGE gel (indicated by the triangle in a lower panel of Fig. 5b) showed that this treatment released certain *N*-glycans from NALM-6 CD10. Desialylation and/or degalactosylation of CD10 molecules was confirmed by lectin blotting with RCA, which binds to lactose and *N*-acetyllactosamine. Binding of RCA to the raft microdomains was reduced by β-galactosidase treatment (Fig. 5c, lane 3), and enhanced by sialidase treatment (lane 4). The enhancement of RCA binding by desialylation was canceled by degalactosylation (lane 5). These results show that sialidase treatment successfully removed sialic acids at the non-reducing end and exposed LacNAc residues, and that the further

Table 1
Results of glycosylation analysis of *N*-glycans of NALM-6 CD10.

Peak no	Observed mass (charge)	Monoisotopic mass (charge)	Composition[a]	Deduced structure[b]
1	866.32(2)	1730.624	[Hex]5[HexNAc]3[NeuAc]1	Hybrid
2	785.30(2)	1568.571	[Hex]4[HexNAc]3[NeuAc]1	Hybrid
3	1399.52(1), 700.26(2)	1560.555	[Hex]7[HexNAc]2	M7
3	1561.58(1), 781.29(2)	1398.502	[Hex]6[HexNAc]2	M6
4	947.35(2)	1892.677	[Hex]6[HexNAc]3[NeuAc]1	Hybrid
5	1113.41(2)	2224.799	[Hex]5[HexNAc]4[NeuAc]2	BiNA2
6	967.86(2)	1933.703	[Hex]5[HexNAc]4[NeuAc]1	BiNA
6	939.36(2)	1876.682	[Hex]5[HexNAc]3[NeuAc]1[Fuc]1	Hybrid
7	822.32(2)	1642.608	[Hex]5[HexNAc]4	Bi
8	1150.43(2)	2298.835	[Hex]6[HexNAc]5[NeuAc]1	TriNA1
9	1186.45(2)	2370.857	[Hex]5[HexNAc]4[NeuAc]2[Fuc]1	FBiNA2
10	1186.45(2)	2370.857	[Hex]5[HexNAc]4[NeuAc]2[Fuc]1	FBiNA2
11	1237.47(1)	1236.449	[Hex]5[HexNAc]2	M5
11	1040.90(2)	2079.761	[Hex]5[HexNAc]4[NeuAc]1[Fuc]1	FBiNA
12	1040.89(2)	2079.761	[Hex]5[HexNAc]4[NeuAc]1[Fuc]1	FBiNA
13	1223.47(2)	2444.893	[Hex]6[HexNAc]5[NeuAc]1[Fuc]1	FTriNA1
13	1113.42(2)	2224.799	[Hex]5[HexNAc]4[NeuAc]2	BiNA2
14	895.35(2)	1788.666	[Hex]5[HexNAc]4[Fuc]1	FBi
14	1333.01(2), 889.00(3)	2663.968	[Hex]7[HexNAc]6[NeuAc]1	TetraNA1
14	1295.99(2), 864.32(3)	2589.931	[Hex]6[HexNAc]5[NeuAc]2	TriNA2
15	1369.02(2), 913.01(3)	2735.989	[Hex]6[HexNAc]5[NeuAc]2[Fuc]1	FTriNA2
15	1295.98(2), 864.32(3)	2589.931	[Hex]6[HexNAc]5[NeuAc]2	BiLAc1NA2
15	1077.91(2)	2153.798	[Hex]6[HexNAc]5[Fuc]1	FBiLac1
15	1478.55(2), 986.04(3)	2955.063	[Hex]7[HexNAc]6[NeuAc]2	(MS only)
16	1333.01(2), 889.00 (3)	2663.968	[Hex]7[HexNAc]6[NeuAc]1	TriLac1NA1
16	1514.56(2), 1010.04(3)	3027.084	[Hex]6[HexNAc]5[NeuAc]3[Fuc]1	FTriNA3
16	1295.98(2), 864.32(3)	2589.931	[Hex]6[HexNAc]5[NeuAc]2	(MS only)
16	1150.44(2)	2298.835	[Hex]6[HexNAc]5[NeuAc]1	BiLac1NA1
17	1186.45(2)	2370.857	[Hex]5[HexNAc]4[NeuAc]2[Fuc]1	FBiNA2
17	1223.47(2)	2444.893	[Hex]6[HexNAc]5[NeuAc]1[Fuc]1	FTriNA1
18	1551.59(2), 1034.72(3)	3101.121	[Hex]7[HexNAc]6[NeuAc]2[Fuc]1	FTetraNA2
18	1406.04(2), 937.69(3)	2810.026	[Hex]7[HexNAc]6[NeuAc]1[Fuc]1	FTetraNA1
18	1369.02(2), 913.01(3)	2735.989	[Hex]6[HexNAc]5[NeuAc]2[Fuc]1	FBiLac1NA2
18	1478.56(2), 986.04(3)	2955.063	[Hex]7[HexNAc]6[NeuAc]2	(MS only)
19	1333.01(2), 889.00(3)	2663.968	[Hex]7[HexNAc]6[NeuAc]1	TriLac1NA1
19	1223.47(2), 815.98(3)	2444.893	[Hex]6[HexNAc]5[NeuAc]1[Fuc]1	FBiLac1NA1
20	1406.04(2), 937.69(3)	2810.026	[Hex]7[HexNAc]6[NeuAc]1[Fuc]1	FTriLac1NA1 or FBiLac2NA1
20	1369.02(2), 913.01(3)	2735.989	[Hex]6[HexNAc]5[NeuAc]2[Fuc]1	FBiLac1NA2
21	1734.16(2), 1156.44(3)	3466.253	[Hex]8[HexNAc]7[NeuAc]2[Fuc]1	FTetraLac1NA2 or FTriLac2NA2
21	1697.14(2), 1131.75(3)	3392.216	[Hex]7[HexNAc]6[NeuAc]3[Fuc]1	FTriLac1NA3
21	1551.59(2), 1034.72(3)	3101.121	[Hex]7[HexNAc]6[NeuAc]2[Fuc]1	FTriLac1NA2
21	1478.55(2), 986.04(3)	2955.063	[Hex]7[HexNAc]6[NeuAc]2	(MS only)
21	1260.49(2), 840.66(3)	2518.930	[Hex]7[HexNAc]6[Fuc]1	FTriLac1 or FBiLac2
21	1406.04(2)	2810.026	[Hex]7[HexNAc]6[NeuAc]1[Fuc]1	FTriLac1NA1 or FBiLac2NA1
22	1588.61(2), 1059.40(3)	3175.158	[Hex]8[HexNAc]7[NeuAc]1[Fuc]1	FTetraLac1NA1 or FTriLac2NA1
22	1406.04(2)	2810.026	[Hex]7[HexNAc]6[NeuAc]1[Fuc]1	FTriLac1NA1 or FBiLac2NA1
23	1375.18(3)	4122.481	[Hex]9[HexNAc]8[NeuAc]3[Fuc]1	FTetraLac2NA3 or FTriLac3NA3
23	1734.16(2), 1156.43(3)	3466.253	[Hex]8[HexNAc]7[NeuAc]2[Fuc]1	FTetraLac1NA2 or FTriLac2NA2
23	1551.59(2), 1034.72(3)	3101.121	[Hex]7[HexNAc]6[NeuAc]2[Fuc]1	FTriLac1NA2
24	1278.15(3)	3831.385	[Hex]9[HexNAc]8[NeuAc]2[Fuc]1	FTetraLac2NA2 or FTriLac3NA2
24	1588.61(2), 1059.40(3)	3175.158	[Hex]8[HexNAc]7[NeuAc]1[Fuc]1	FTetraLac1NA1 or FTriLac2NA1
24	1406.03(2)	2810.026	[Hex]7[HexNAc]6[NeuAc]1[Fuc]1	(MS only)
25	1181.12(3)	3540.290	[Hex]9[HexNAc]8[NeuAc]1[Fuc]1	FTetraLac2NA1 or FTriLac3NA1
25	1375.19(3)	4122.481	[Hex]9[HexNAc]8[NeuAc]3[Fuc]1	(MS only)

[a] Estimated from m/z values obtained by FTMS.
[b] Deduced from MS^n spectra in positive ion mode; F, fucose; NA, *N*-acetylneuraminic acid; Lac, LacNAc; Bi, biantennary; Tri, triantennary; Tetra, tetraantennary.

treatment with β-galactosidase certainly removed β-galactose residues that had been exposed by the sialidase treatment.

Desialylation and/or degalactosylation of the raft microdomains reduced NEP activities to 80–90% of untreated NEP (Fig. 5d, lanes 2, 3, and 4), whereas glycopeptidase F treatment under non-denaturing conditions greatly reduced NEP activities, although this treatment did not change the MW of CD10 (Fig. 5d, lane 5). Treatment of purified CD10 of NALM-6 cells with glycopeptidase F under non-denaturing conditions also suppressed NEP activities (Fig. 5e). These results show that a certain *N*-glycan, which can be easily digested by glycopeptidase F even under non-denaturing conditions, is necessary for full expression of NEP activities.

3.5. Expression of CD10 lacking N-glycan in HEK 293 cells

To examine which *N*-glycans are required for expression of NEP activities, we constructed mutated CD10 lacking *N*-glycans as shown in Fig. 1, and expressed the mutated CD10 in HEK293 cells. Surface expressions of WT and mutated CD10 on HEK293 cells were examined by flow cytometry and Western analysis. WT, Δ1, and Δ2CD10 were fully expressed on the surface of HEK293 cells, but Δ3CD10 was hardly expressed (Fig. 6a). Western analysis confirmed strong expression of WT, Δ1, and Δ2CD10 and weak expression of Δ3CD10 (Fig. 6b). However, transcription of all of these 4 lines occurred at the same level (Fig. 6c). Reduction in molecular weight of WT and mutated CD10 by

Table 2
Nucleotide sequences of oligonucleotide primers used for amplifying, sequencing and site-directed mutagenesis of NALM-6 CD10.

Primer name	Primer sequence (5′ to 3′)
Cloning_sense	5′-gatgggcaagtcagaaagtcagatgg-3′
Cloning_antisense	5′-caaacccggcacttcttttctggat-3′
Seq._sense	5′-gagatcaatgggaagccattcagctgg-3′
Seq._antisense	5′-gaggctgcttacaagatccattatg-3′
N145Q_sense	5′-agcaaaagcattgtacaggtcttgtatacaggaatctgctattgatagcag-3′
N145Q_antisense	5′-ctgctatcaatagcagattcctgtatacaagacctgtacaatgcttttgct-3′
N325Q_sense	5′-gggaagccattcagctggttgcagttcacaaatgaaatcatgtcaa-3′
N325Q_antisense	5′-ttgacatgatttcatttgtggaactgcaaccagctgaatggcttccc-3′
N628Q_sense	5′-catggtgtatcagtatggacagttttcctgggacctggcag-3′
N628Q_antisense	5′-ctgccaggtcccaggaaaactgtccatactgatacaccatg-3′

glycopeptidase F treatment indicates the presence of *N*-glycans in these CD10 molecules (Fig. 6d).

3.6. NEP activities of WT and mutated CD10

The amounts of MCA (nmol) released by 5×10^4 HEK293 cells transfected with WT-, Δ1-, Δ2-, and Δ3-CD10 were 2.34, 0.39, 1.10, and 0.06, respectively (Fig. 7a). Since the expression level of CD10 varied among transfectants, we examined the NEP activities of CD10 purified from transfectants by immunoprecipitation. The amount of CD10 was determined by Western analysis of the immunoprecipitates, which were separated by 2D PAGE (Fig. 7b). We detected NEP activities in the immunoprecipitates from WT-, Δ1-, and Δ2-CD10 transfectants, but not any activities in that of Δ3-CD10 transfectant (Fig. 7c). These results show that CD10 lacking an *N*-glycan at N_{628} is defective not only in surface expression, but also in expression of NEP catalytic activities.

3.7. Effects of inhibition of intracellular traffic on the protein expression of CD10

In order to elucidate in which step the protein expression of Δ3CD10 is suppressed, we cultured human B-cell lines of NALM-6 and Reh and transfectants of WT- and Δ3-CD10 in the presence of brefeldin A or lactacystin, and examined their expression by Western analysis. Brefeldin A inhibits transport from ER to Golgi apparatus, resulting in avoidance of degradation in a lysosome [25], and lactacystin inhibits proteasome activity [26]. CD10 molecules having an MW of more than a few hundred thousand were detected in NALM-6 cells cultured in the presence of lactacystin (open arrow in Fig. 8a). The amount of CD10 decreased and increased in Reh cells cultured in the presence of brefeldin A and lactacystin (closed and open arrowheads in Fig. 8a), respectively. Aggregated CD10 of NALM-6 or misfolded CD10 of Reh seems to be digested in proteasome, and inhibition of transport from ER to Golgi apparatus suppresses the expression of CD10 of Reh. HEK293 cells transfected with WT-CD10 decreased and increased the expression during the culture in the presence of brefeldin A and lactacystin, respectively (closed and open arrowheads in Fig. 8b), whereas those with Δ3-CD10 increased the expression during the culture in the presence of brefeldin A (asterisk in Fig. 8b) and did not increase the expression during the culture in the presence of lactacystin. Next, we used chloroquine to inhibit lysosmal proteases [27]. The amount of Δ3-CD10 was not increased by the treatment with either lactacystin or chloroquine (Fig. 8c). These results indicate that the low level of expression of Δ3-CD10 in HEK293 cells may not be due to degradation either in proteasome or lysosomes.

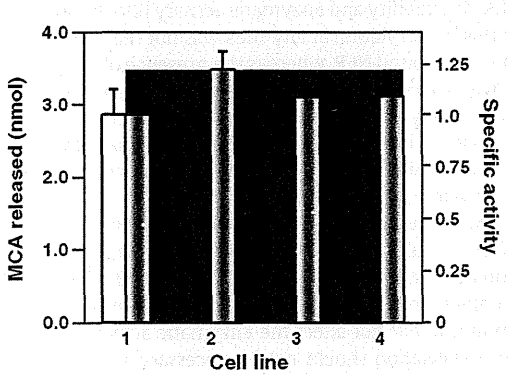

Fig. 4. NEP activities of human B-cell lines. The open column represents nmol MCA released by 5×10^4 cells into 50 μL of the assay buffer for 30 min and the solid column represents the specific activity. The specific activity was calculated as follows: nmol MCA released was divided by the arbitrary unit of CD10 in a test tube, and the value for Reh was set to 1.0. 1, Reh; 2, NALM-16; 3, NALM-6; 4, RAMOS. Error bars mean SD values of triplicate measurements.

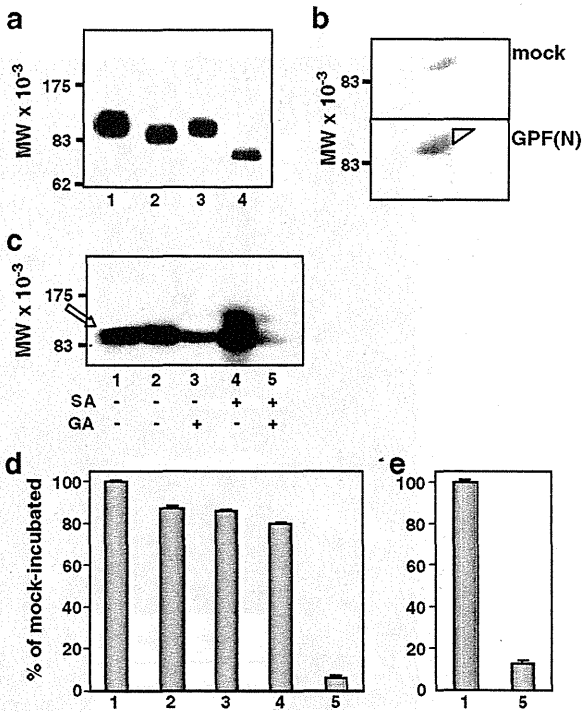

Fig. 5. Effects of glycosidase treatment on NEP activities of NALM-6 cells. a, Reduction in MW of CD10 of the glycosidase-treated raft microdomain. The raft microdomain (4 μg each) was mock-incubated or incubated with glycosidases for 16 h, and then subjected to Western blot analysis with anti-CD10. 1, Mock-incubated; 2, sialidase; 3, glycopeptidase F under non-denaturing conditions; 4, glycopeptidase F under denaturing conditions. b, 2D PAGE of the glycosidase-treated CD10. 12 μg of protein of mock-incubated (mock, upper panel) and glycopeptidase F-treated raft under non-denaturing conditions (GPF(N), lower panel) were subjected to 2D PAGE. 2D gels were silver-stained. The triangle indicates an area which disappeared after glycopeptidase F treatment under non-denaturing conditions. c, RCA lectin binding to the glycosidase-treated raft microdomain. The raft microdomain (4 μg each) was mock-incubated or incubated with glycosidases, and then subjected to lectin-blot analysis with RCA lectin. 1, Mock-incubated for 7 h; 2, mock-incubated for 20 h; 3, β-galactosidase (GA) for 7 h; 4, sialidase (SA) for 13 h; 5, sialidase for 13 h and then β-galactosidase for 7 h; open arrow indicates CD10. d, NEP activities of the glycosidase-treated raft microdomains. e, NEP activities of the glycosidase-treated CD10. Percentages of NEP activities of the glycosidase-treated to that of the mock-incubated are shown. 1, Mock-incubated; 2, sialidase; 3, β-galactosidase; 4, sialidase and then β-galactosidase; 5, glycopeptidase F under non-denaturing conditions.

4. Discussion

As we presented in this study, CD10 of human BCP-ALL cell line is one of the major raft micodomain glycoproteins and heterogeneously

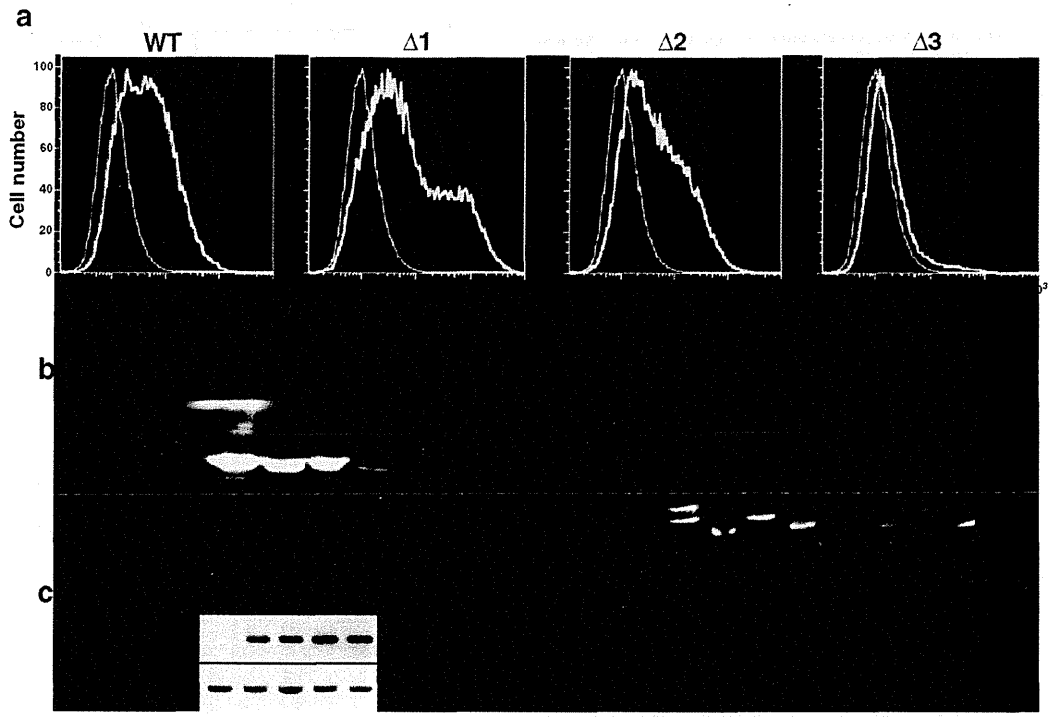

Fig. 6. Expression and glycosylation of CD10 in HEK293 cells transfected with wild type and mutated c-DNA of NALM-6 CD10. a, Surface expression of CD10 by the transfected HEK293 cells. HEK293 cells were harvested at day 2 after transfection and their expression of CD10 was analyzed by flow cytometry. Thin line, negative control; bold line, IF6. b, Protein expression of CD10 by transfected HEK 293 cells. 2×10^5 transfectants were solubilized and subjected to Western analysis with anti-CD10. c, RT-PCR analysis of CD10 and GAPDH mRNA expression. d, *N*-glycosylation of WT- and mutated CD10. Each lysate was mock-incubated (GPF−) or incubated with glycopeptidase F (GPF+) under denaturing conditions, and subjected to Western analysis with anti-CD10. Lanes 2, 3, 4 and lane 5 contain 3×10^5 and 6×10^5 cells, respectively. 1, Vector; 2, WT: 3, Δ1; 4, Δ2; 5, Δ3.

N-glycosylated. It is suggested that *N*-glycans are necessary for full expression of NEP activities because of the complete loss of NEP activities upon glycopeptidase F treatment. Interestingly, site-directed mutagenesis of *N*-glycosylation sites of CD10 reveals that an *N*-glycan at Asn_{628} is indispensable not only for NEP activities but also for surface expression. The proteins of Δ3-CD10 lacking an *N*-glycan at Asn_{628} seem to be eliminated via a certain protein quality control pathway. Since either lactacystin or chloroquine did not cause the accumulation of Δ3-CD10, the low expression of Δ3-CD10 cannot be explained by the degradation either in proteasome or lysosome. However, Δ3-CD10 transfectants increased the expression upon brefeldin A treatment. The addition of brefeldin A to cells is known to result in the tubulation of the endosomal system, the transe-Golgi network, and lysosomes [28]. It should be cleared how the proteins of Δ3-CD10, which is deficient in NEP activity due to lack of an *N*-glycan at Asn_{628}, are degraded.

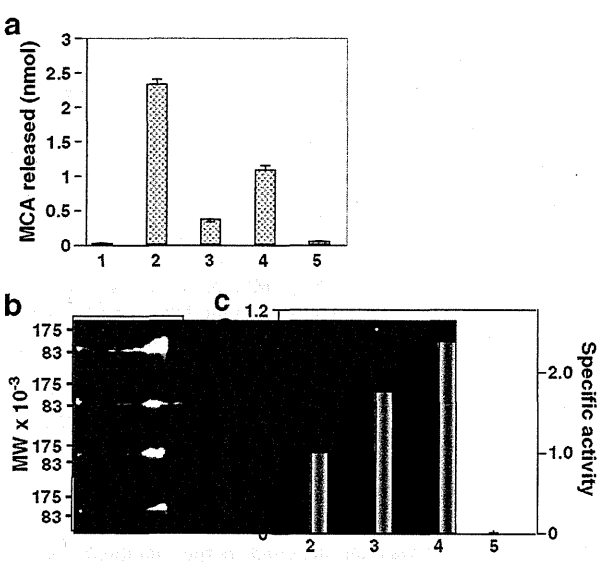

Fig. 7. NEP activities of HEK293 cells transfected with WT or mutated CD10. a, NEP activities of 5×10^4 transfectants. b, 2D Western analysis of CD10 immunoprecipitated from transfectants with anti-CD10. c, NEP activities of CD10 purified from transfectants. CD10 immunoprecipitated from 1.3×10^6 WT-, Δ1-, and Δ2-CD10 transfectants, and 1.7×10^6 Δ3-CD10 transfectants on PA/agarose beads was used as an enzyme source for NEP assay. After that, the beads were subjected to Western analysis with anti-CD10 for determination of the amount of CD10. The open column represents nmol MCA released by 5×10^4 cells into 50 μL of the assay buffer for 30 min and the solid column represents the specific activity. The value for WT-CD10 was set to 1.0. 1, Vector; 2, WT: 3, Δ1; 4, Δ2; 5, Δ3.

Previous studies have shown that changes in *N*-glycans of rabbit NEP affect its stability and enzymatic activity [29]. It has been demonstrated that glycosylation at any sites was not required for expression of membrane-bound NEP, whereas the presence of *N*-glycans at either N_{145} or N_{628} was sufficient to recover close-to-normal enzymatic activities. In our study, *N*-glycans at N_{628} of human membrane-bound CD10 were revealed to be necessary not only for expression, but also for enzymatic activities, whereas *N*-glycans at N_{145} were nonessential for both expression and enzymatic activities.

The experimental removal of sialic acid by *Vibrio cholerae* neuraminidase in cultured myotubes was shown to result in reduced expression and enzymatic activity of NEP in vitro [30]. We demonstrated that complete removal of sialic acid by *Anthrobacter ureafaciens* neuraminidase did not affect the enzymatic activity of human CD10. Therefore, sialylation should not be necessary at least for enzymatic activity.

Although the transcription level of Δ3-CD10 was almost the same as that of WT or other mutants, its surface expression was extremely low compared with that of the others. We have to keep in mind that quantification of the mRNA of CD10 does not reflect the protein expression or catalyzing activity of NEP.

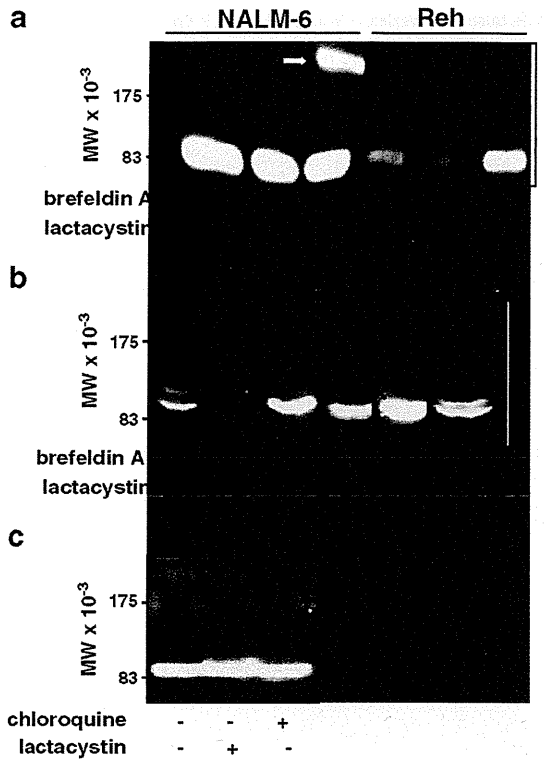

Fig. 8. Effect of brefeldin A, lactacystin and chloroquine on the expression of CD10. a, Cells were cultured in the presence or absence of brefeldin A or lactacystin, and harvested for Western analysis. Each lane contains 14 μg of protein of NALM-6 and Reh. b, 3×10^5 WT- and 6×10^5 Δ3-CD10 transfectants were loaded. c, 8×10^5 Δ3-CD10 transfectants were cultured in the presence or absence of lactacystin or brefeldin A, and harvested for Western analysis.

Abbreviations

NEP	neutral endopeptidase
ALL	acute lymphoblastic leukemia
CALLA	common acute lymphoblastic leukemia antigen
WT	wild type
mAb	monoclonal antibody
2D	two dimensional
PBS	phosphate-buffered saline
CBB	Coomassie brilliant blue
MCA	4-methyl-coumaryl-7-amides
pI	isoelectric point

Acknowledgements

This work was supported by the Health and Labour Sciences Research Grants (the 3rd-term comprehensive 10-year strategy for cancer control H22-011), the Grant of the National Center for Child Health and Development (22A-5), and the Program for Promotion of Fundamental Studies in Health Sciences of the National Institute of Biomedical Innovation (NIBIO, 10–41, -42, -43, -44, -45).

References

[1] M.F. Greaves, G. Hariri, R.A. Newman, D.R. Sutherland, M.A. Ritter, J. Ritz, Selective expression of the common acute lymphoblastic leukemia (gp 100) antigen on immature lymphoid cells and their malignant counterparts, Blood 61 (1983) 628–639.
[2] K. Tsuganezawa, N. Kiyokawa, Y. Matsuo, F. Kitamura, N. Toyama-Sorimachi, K. Kuida, J. Fujimoto, H. Karasuyama, Flow cytometric diagnosis of the cell lineage and developmental stage of acute lymphoblastic leukemia by novel monoclonal antibodies specific to human pre-B-cell receptor, Blood 92 (1998) 4317–4324.
[3] N. Kiyokawa, Y. Kokai, H. Fujita, K. Ishimoto, J. Fujimoto, J. Hata, Characterization of the common acute lymphoblastic leukaemia antigen (CD10) as an activation molecule on mature human B cells, Clin. Exp. Immunol. 79 (1990) 322–327.
[4] R.S. Metzgar, M.J. Borowitz, N.H. Jones, B.L. Dowell, Distribution of common acute lymphoblastic leukemia antigen in nonhematopoietic tissues, J. Exp. Med. 154 (1981) 1249–1254.
[5] M.P. Braun, P.J. Martin, J.A. Ledbetter, J.A. Hansen, Granulocytes and cultured human fibroblasts express common acute lymphoblastic leukemia-associated antigens, Blood 61 (1983) 718–725.
[6] M.A. Shipp, J. Vijayaraghavan, E.V. Schmidt, E.L. Masteller, L. D'Adamio, L.B. Hersh, E.L. Reinherz, Common acute lymphoblastic leukemia antigen (CALLA) is active neutral endopeptidase 24.11 ("enkephalinase"): direct evidence by cDNA transfection analysis, Proc. Natl. Acad. Sci. U. S. A. 86 (1989) 297–301.
[7] E.G. Erdös, R.A. Skidgel, Neutral endopeptidase 24.11 (enkephalinase) and related regulators of peptide hormones, FASEB J. 3 (1989) 145–151.
[8] Y. Takaki, N. Iwata, S. Tsubuki, S. Taniguchi, S. Toyoshima, B. Lu, N.P. Gerard, C. Gerard, H.J. Lee, K. Shirotani, T.C. Saido, Biochemical identification of the neutral endopeptidase family member responsible for the catabolism of amyloid beta peptide in the brain, J. Biochem. 128 (2000) 897–902.
[9] B. Lu, N.P. Gerard, L.F. Kolakowski Jr., M. Bozza, D. Zurakowski, O. Finco, M.C. Carroll, C. Gerard, Neutral endopeptidase modulation of septic shock, J. Exp. Med. 181 (1995) 2271–2275.
[10] B.P. Roques, F. Noble, V. Daugé, M.C. Fournié-Zaluski, A. Beaumont, Neutral endopeptidase 24.11: structure, inhibition, and experimental and clinical pharmacology, Pharmacol. Rev. 45 (1993) 87–146.
[11] E. Bachelard-Cascales, M. Chapellier, E. Delay, G. Pochon, T. Voeltzel, A. Puisieux, C. Caron de Fromentel, V. Maguer-Satta, The CD10 enzyme is a key player to identify and regulate human mammary stem cells, Stem Cells 28 (2010) 1081–1088.
[12] Y.U. Katagiri, K. Ohmi, C. Katagiri, T. Sekino, H. Nakajima, T. Ebata, N. Kiyokawa, J. Fujimoto, Prominent immunogenicity of monosialosyl galactosylgloboside, carrying a stage-specific embryonic antigen-4 (SSEA-4) epitope in the ACHN human renal tubular cell line-a simple method for producing monoclonal antibodies against detergent-insoluble microdomains/raft, Glycoconj. J. 18 (2001) 347–353.
[13] Y.U. Katagiri, K. Ohmi, W. Tang, H. Takenouchi, T. Taguchi, N. Kiyokawa, J. Fujimoto, Raft.1, a monoclonal antibody raised against the raft microdomain, recognizes G-protein β1 and 2, which assemble near nucleus after shiga toxin binding to human renal cell line, Lab. Invest. 82 (2002) 1735–1745.
[14] T. Taguchi, N. Kiyokawa, K. Mimori, T. Suzuki, T. Sekino, H. Nakajima, M. Saito, Y.U. Katagiri, N. Matsuo, Y. Matsuo, H. Karasuyama, J. Fujimoto, Pre-B cell antigen receptor-mediated signal inhibits CD24-induced apoptosis in human pre-B cells, J. Immunol. 170 (2003) 252–260.
[15] T. Suzuki, N. Kiyokawa, T. Taguchi, T. Sekino, Y.U. Katagiri, J. Fujimoto, CD24 induces apoptosis in human B cells via the glycolipid-enriched membrane domains/rafts-mediated signaling system, J. Immunol. 166 (2001) 5567–5577.
[16] A. Helenius, M. Aebi, Roles of N-linked glycans in the endoplasmic reticulum, Annu. Rev. Biochem. 73 (2004) 1019–1049.
[17] C. Oefner, A. D'Arcy, M. Hennig, F.K. Winkler, G.E. Dale, Structure of human neutral endopeptidase (Neprilysin) complexed with phosphoramidon, J. Mol. Biol. 296 (2000) 341–349.
[18] J. Fujimoto, K. Ishimoto, N. Kiyokawa, S. Tanaka, E. Ishii, J. Hata, Immunocytological and immunochemical analysis on the common acute lymphoblastic leukemia antigen (CALLA): evidence that CALLA on ALL cells and granulocytes are structurally related, Hybridoma 7 (1988) 227–236.
[19] Y.U. Katagiri, N. Kiyokawa, K. Nakamura, H. Takenouchi, T. Taguchi, H. Okita, A. Umezawa, J. Fujimoto, Laminin binding protein, 34/67 laminin receptor, carries stage-specific embryonic antigen-4 epitope defined by monoclonal antibody Raft.2, Biochem. Biophys. Res. Commun. 332 (2005) 1004–1011.
[20] M. Kikuchi, N. Hatano, S. Yokota, N. Shimozawa, T. Imanaka, H. Taniguchi, Proteomic analysis of rat liver peroxisome: presence of peroxisome-specific isozyme of Lon protease, J. Biol. Chem. 279 (2004) 421–428.
[21] B. Küster, S.F. Wheeler, A.P. Hunter, R.A. Dwek, D.J. Harvey, Sequencing of N-linked oligosaccharides directly from protein gels: in-gel deglycosylation followed by matrix-assisted laser desorption/ionization mass spectrometry and normal-phase high-performance liquid chromatography, Anal. Biochem. 250 (1997) 82–101.
[22] I. Morita, S. Kakudaa, Y. Takeuchi, S. Itoh, N. Kawasaki, Y. Kizuka, T. Kawasaki, S. Oka, HNK-1 glyco-epitope regulates the stability of the glutamate receptor subunit GluR2 on the neutral cell surface, J. Biol. Chem. 284 (2009) 30209–30217.
[23] T. Ogawa, S. Kiryu-Seo, M. Tanaka, H. Konishi, N. Iwata, T. Saido, Y. Watanabe, H. Kiyama, Altered expression of neprilysin family members in the pituitary gland of sleep-disturbed rats, an animal model of severe fatigue, J. Neurochem. 95 (2005) 1156–1166.
[24] S. Voisin, D. Rognan, C. Gros, T. Ouimet, A three-dimensional model of the neprilysin 2 active site based on the X-ray structure of neprilysin. Identification of residues involved in substrate hydrolysis and inhibitor binding of neprilysin 2, J. Biol. Chem. 279 (2004) 46172–46181.
[25] E.S. Liu, J-h. Ou, A.S. Lee, Brefeldin A as a regulator of grp78 gene expression in mammalian cells, J. Biol. Chem. 267 (1992) 7128–7133.
[26] K. Kawana, A.J. Quayle, M. Ficarra, J.A. Ibana, L. Shen, Y. Kawana, H. Yang, L. Marrero, S. Yavagal, S.J. Greene, Y.X. Zhang, R.B. Pyles, R.S. Blumberg, D.J. Schust, CD1d degradation in Chlamydia trachomatis-infected epithelial cells is the result of both cellular and chlamydial proteasomal activity, J. Biol. Chem. 282 (2007) 7368–7375.

[27] K.C. Walls, A.P. Ghosh, A.V. Franklin, B.J. Klocke, M. Ballestas, J.J. Shacka, J. Zhang, K.A. Roth, Lysosome dysfunction triggers Atg7-dependent neural apoptosis, J. Biol. Chem. 285 (2010) 10497–10507.
[28] J. Lippincott-Schwartz, L. Yuan, C. Tipper, M. Amherdt, L. Orci, R.D. Klausner, Brefeldin A's effects on endosomes, lysosomes, and the TGN suggest a general mechanism for regulating organelle structure and membrane traffic, Cell 67 (1991) 601–616.
[29] M.H. Lafrance, C. Vézina, Q. Wang, G. Boileau, P. Crine, G. Lemay, Role of glycosylation in transport and enzymic activity of neutral endopeptidase-24.11, Biochem. J. 302 (1994) 451–454.
[30] A. Broccolini, T. Gidaro, R. De Cristofaro, R. Morosetti, C. Gliubizzi, E. Ricci, P.A. Tonali, M. Mirabella, Hyposialylation of neprilysin possibly affects its expression and enzymatic activity in hereditary inclusion-body myopathy muscle, J. Neurochem. 105 (2008) 971–981.

Int J Hematol
DOI 10.1007/s12185-012-1234-3

ORIGINAL ARTICLE

Effects of insulin-like growth factor-1 on B-cell precursor acute lymphoblastic leukemia

Hiroyuki Yamada · Kazutoshi Iijima · Osamu Tomita · Tomoko Taguchi · Masashi Miharu · Kenichiro Kobayashi · Hajime Okita · Masahiro Saito · Toshiaki Shimizu · Nobutaka Kiyokawa

Received: 2 August 2012 / Revised: 26 November 2012 / Accepted: 26 November 2012

Abstract Insulin-like growth factor-1 (IGF-1) is known to be a major growth factor with effects on various cell types, including hematopoietic cells, as well as neoplasms, and is regulated by IGF-binding proteins (IGFBPs). In this study, we investigated the effects of IGF-1 on B-cell precursor acute lymphoblastic leukemia (BCP-ALL) cells. When the expression of IGF-1R in clinical samples of BCP-ALL was examined, five of thirty-two cases showed IGF-1R expression, whereas IGF-1R was expressed in most BCP-ALL cell lines. We observed that IGF-1 enhanced the proliferation of BCP-ALL cell lines that can be partially inhibited by IGFBP-1, -3, and -4, but not other IGFBPs. IGF-1 also partially inhibited dexamethasone-induced apoptosis, but not apoptosis mediated by VP-16 and irradiation. Interestingly, the proliferative effect of IGF-1 was partially blocked by inhibitors of MAPK and AKT, whereas the inhibition of dexamethasone-induced apoptosis was completely blocked by both inhibitors. Our data indicate that IGF-1 is involved in cell proliferation and apoptosis regulation in BCP-ALL cells. Since some BCP-ALL cases express IGF-1R, it appears to be a plausible target for prognostic evaluation and may represent a new therapeutic strategy.

Keywords IGF-1 · IGFBP · B-cell precursor ALL · Cell growth · Apoptosis

Introduction

Insulin-like growth factor-1 (IGF-1) is known to be a major growth factor affecting various types of cell [1]. IGF-1 can bind to the homodimer of IGF-1 receptor (IGF-1R) and the heterodimer of IGF-1R and insulin receptor with different affinities. Upon binding with these receptors, IGF-1 induces intracellular signaling, including Akt and MAPK pathways, leading to the enhancement of cell cycle progression, cell proliferation, and cell differentiation [2, 3]. In regard to neoplastic cells, many studies have provided evidence for roles of IGF-1 in several tumor developments. For example, an elevated plasma concentration of IGF-1 has been shown to be linked to a higher risk of several solid tumors, including bladder [4], breast [5–7], colorectal [5, 8], lung [5, 9], pancreatic [10], and prostate cancer [5, 11], and malignant melanoma [12]. In hematological malignancies, an autocrine effect of IGF-I signaling on the growth and survival of acute myeloid leukemia (AML) cells has been reported [13]. In the case of B-cell precursor acute lymphoblastic leukemia (BCP-ALL) cells, the expression of IGF system components in primary leukemic blasts has been shown [14], whereas its biological significance still remains unclear.

The bioactivity of IGF-1 is known to be modulated by a family of proteins termed IGF binding proteins (IGFBPs). IGFBPs have a high binding affinity for IGF-1, while their effects are variable and some of them limit IGF-1 access to

Electronic supplementary material The online version of this article (doi:10.1007/s12185-012-1234-3) contains supplementary material, which is available to authorized users.

H. Yamada · K. Iijima · O. Tomita · T. Taguchi · M. Miharu · K. Kobayashi · H. Okita · N. Kiyokawa (✉)
Department of Pediatric Hematology and Oncology Research, National Research Institute for Child Health and Development, 2-10-1, Okura, Setagaya-ku, Tokyo, 157-8535, Japan
e-mail: nkiyokawa@nch.go.jp

H. Yamada · O. Tomita · M. Saito · T. Shimizu
Department of Pediatrics and Adolescent Medicine, Juntendo University Graduate School of Medicine, Bunkyo-ku, Tokyo, Japan

Published online: 19 December 2012

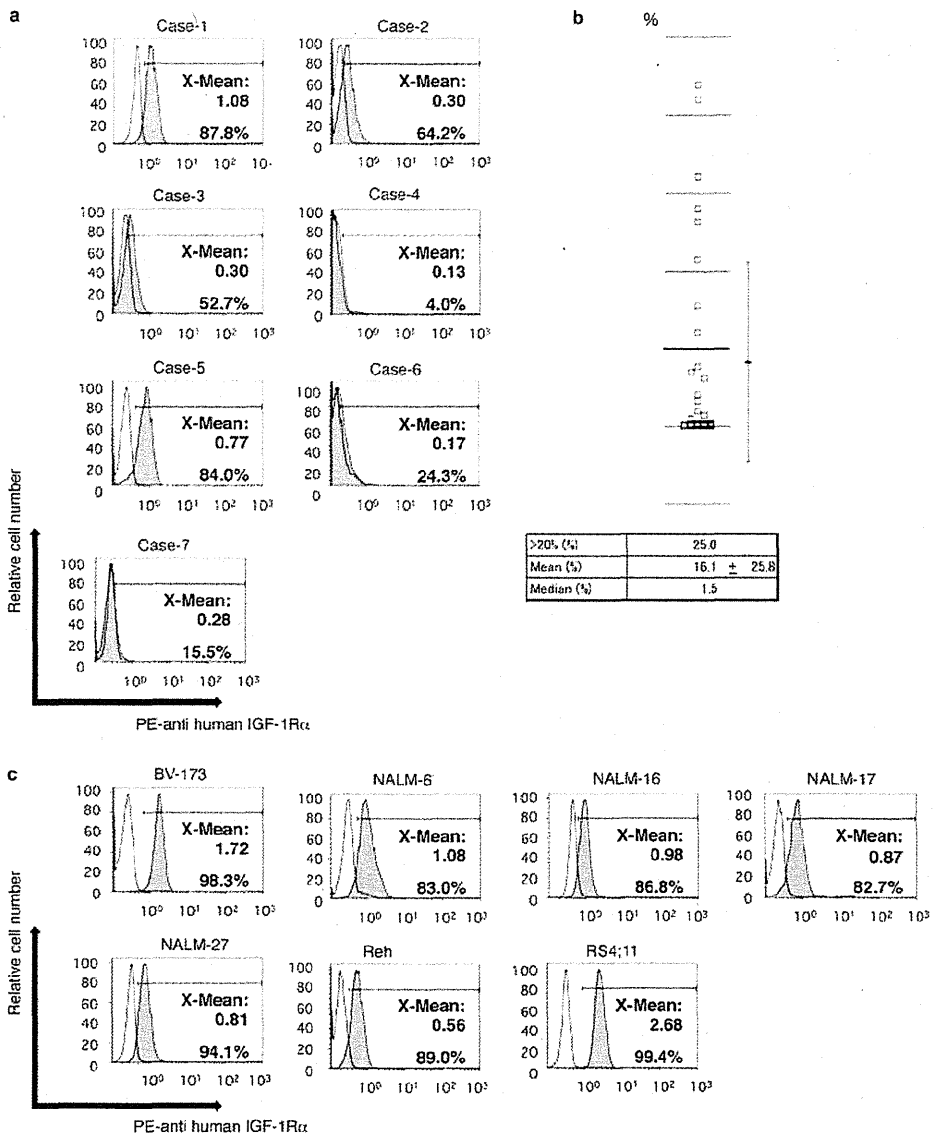

Fig. 1 Expression of insulin-like growth factor-1 receptor (IGF-1R) in B-cell precursor acute lymphoblastic leukemia (BCP-ALL) cells. **a** Leukemic cells obtained from seven patients with BCP-ALL were stained with phycoerythrin (PE)-labeled anti-human IGF-1Rα antibody and analyzed by flow cytometry. **b** IGF-1R positivity (percentage) of BCP-ALL [$n = 32$, including the cases presented in **a**] was plotted on a scattergram. Percentage of IGF-1R -positive cases (more than 20 % expression in blasts) is indicated below. **c** Seven BCP-ALL cell lines were stained and analyzed, as shown in **a**. The histograms obtained (*dark areas*) are shown superimposed on those of the negative control (cells stained with isotype-matched control mouse Ig, light areas, cut-off: 2 %). Positivity (%) and mean fluorescence (X-mean) values are presented. *X*-axis, fluorescence intensity; *Y*-axis, relative cell number

the IGF-1 receptor (IGF-1R) [15], but the others serve as a carrier protein for IGF-1 [16] and help to lengthen the half-life of circulating IGF-1 [17]. We previously reported the regulatory effects of IGF-1 and IGFBPs on early B-cell development by employing an in vitro culture system of human hematopoietic stem cells cocultured with bone marrow stromal cells, and observed that IGF-1 is essential for pro-B-cell development from $CD34^+$ cells and IGFBP-3 inhibited but IGFBP-6 was required for pro-B-cell development [18]. Considering the fact that BCP-ALL cells are tumor counterparts of B-cell precursors, IGF-1 and IGFBPs should play an important role in the biology of ALL cells.

In the present report, we investigated the functions of IGF-1 and IGFBPs in the proliferation and survival of BCP-ALL cells. We show that IGF-1 promotes the proliferation of BCP-ALL cells and inhibits apoptosis under specific circumstances. The effects of IGFBPs on ALL cells were also shown.

Methods

Reagents

The antibodies (Abs) used for flow cytometry were phycoerythrin (PE)-conjugated mouse monoclonal anti-human IGF-1 Rα from Becton Dickinson Biosciences (BD, San Diego, CA, USA), Alexa Fluor® 488-conjugated rabbit

polyclonal anti-Phospho-p44/41 mitogen-activated protein kinase (MAPK) (Thr202/Tyr204), and Alexa Fluor® 488-conjugated rabbit monoclonal anti-Phospho-Akt (Ser473) from Cell Signaling Technology, Inc. (Danvers, MA, USA). The antibodies (Abs) used for immunoblot analysis were mouse monoclonal anti-ERK antibody and anti-Akt antibody from BD, anti-IGF-1R antibody, anti-phospho-IGF-1R antibody, anti-phospho-p44/42-MAPK antibody, and anti-Phospho-Akt antibody from Cell Signaling Technology, Inc. As a negative control, isotype-matched control Igs were also used.

Recombinant human IGF-1, IGFBP-2, IGFBP-7, and rabbit anti-human IGF-1 antibody for neutralization were obtained from PeproTech EC Ltd. (London, UK). Recombinant human IGFBP-1 was obtained from R&D SYSTEMS (Minneapolis, MN, USA), IGFBP-3, -4, and -5 were obtained from Sigma-Aldrich, Co. (St. Louis, MO, USA) and IGFBP-6 was obtained from G-T Research Products (Minneapolis, MN, USA). The IGF-1R kinase inhibitor I-OMe-AG538 and the MAPK extracellular signal-regulated kinase (MEK) 1/2 inhibitor U0126 were obtained from Calbiochem-Novabiochem Co. (San Diego, CA, USA). The Phosphoinositide 3-kinase (PI3K) inhibitor LY294002 was obtained from Cell Signaling Technology, Inc. Dexamethasone (DEX) and etoposide (VP-16) were obtained from Sigma-Aldrich.

Clinical specimens

Clinical specimens from pediatric patients, consisting of thirty-two patients with BCP-ALL, were used upon obtaining informed consent. All of the experiments included in this study adhered to the tenets of the Declaration of Helsinki and were performed with the approval of the local ethics committee.

Cells and cultures

The human BCP-ALL cell lines BV-173, NALM-16, NALM-17, and NALM-27 (Dr. Y. Matsuo, Hayashibara Biochemical Laboratories, Inc. Research Center Cell Biology Institute, Okayama, Japan), NALM-6 (Tohoku University Cell Bank, Sendai, Japan), Reh (American Type Culture Collection), and RS4;11 (Japanese Cancer Research Resource Bank, JCRB, Tokyo, Japan) were used. Cells were maintained in RPMI-1640 supplemented with

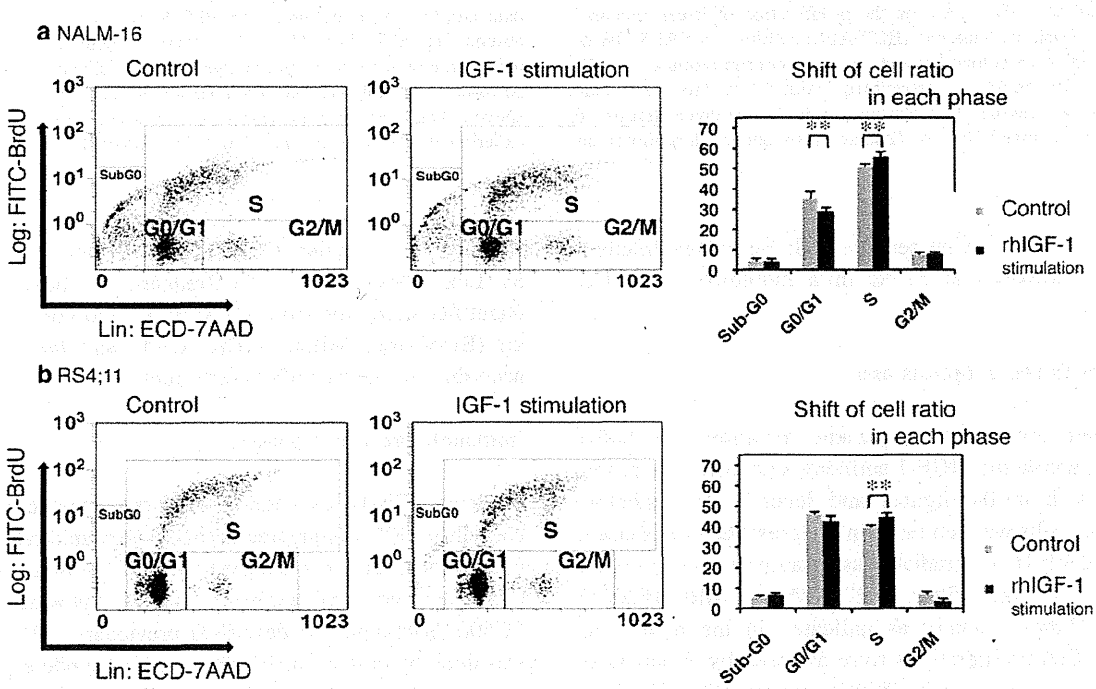

Fig. 2 Effect of insulin-like growth factor-1 (IGF-1) stimulation on cell cycle progression. NALM-16 and RS4;11 cells at a starting cell concentration of 5×10^5 cells/mL with the serum-free condition were incubated with or without 100 ng/mL of IGF-1 for 24 h followed by 4-h labeling with bromodeoxyuridine (BrdU). After staining with fluorescein isothiocyanate (FITC)-labeled (*X*-axis) anti-BrdU antibody and 7-amino-actinomycinD (7AAD, *Y*-axis), cells were analyzed with flow cytometry. Experiments were performed in triplicate, and the mean ± SD of the percentage of each fraction are shown. Data are representative of at least three independent experiments. **significant ($p < 0.05$)